

Dr. Nathalie Combourieu-Nebout, Editor Climate of the Past (Ref. cp-2018-35)

Dear Nathalie,

Thank so much for considering the resubmission of our manuscript entitled "*Vegetation and geochemical responses to Holocene rapid climate change in Sierra Nevada (SE Iberia): The Laguna Hondera record*" authored by J. M. Mesa-Fernández, G. Jiménez-Moreno, M. Rodrigo-Gámiz, A. García-Alix, F. J. Jiménez-Espejo, R. Scott Anderson, F. Martínez-Ruiz, J. Camuera and M. J. Ramos-Román.

We have gone in detail over all the very constructive suggestions that the two reviewers made, which improved our manuscript to a much stronger paper. The amendments are presented in track changes mode.

Yours sincerely,

Jose Manuel Mesa Fernández

Instituto Andaluz de Ciencias de la Tierra (IACT-CSIC)

Av. de las Palmeras, 4 18100 Armilla (Granada)

Vegetation and geochemical responses to Holocene rapid climate change in Sierra Nevada (SE Iberia): The Laguna Hondera record

Jose Manuel Mesa-Fernández^{1, 2}, Gonzalo Jiménez-Moreno¹, Marta Rodrigo-Gámiz², Antonio García-Alix^{1,2}, Francisco J. Jiménez-Espejo³, Francisca Martínez-Ruiz², R. Scott Anderson⁴, Jon Camuera¹ and María J. Ramos-Román¹

¹ Departamento de Estratigrafía y Paleontología, Universidad de Granada (UGR), Avda. Fuente Nueva s/n, 18002, Granada, Spain

² Instituto Andaluz de Ciencias de la Tierra (IACT), CSIC-UGR, Avenida de las Palmeras 4, 18100, Armilla, Granada, Spain

³ Department of Biogeochemistry (JAMSTEC), Yokosuka, Japan.

⁴ School of Earth Sciences and Environmental Sustainability, Northern Arizona University, Flagstaff, AZ, USA.

Correspondance to: Jose Manuel Mesa-Fernández (jmesa@iact.ugr-csic.es)

Abstract.

High-altitude peat bogs and lacustrine records are very sensitive to climate changes and atmospheric dust input. Recent studies have shown a close relationship between regional climate aridity and enhanced eolian input to lake sediments. However, changes in regional-scale dust fluxes due to climate variability at short-scales and how alpine environments were impacted by climatic- and human-induced environmental changes are not completely understood.

Here we present a multi-proxy ([palynological, geochemical and magnetic susceptibility](#)) lake sediment record of climate variability in the Sierra Nevada (SE Iberian Peninsula) over the Holocene. ~~Palynological, geochemical and magnetic susceptibility (MS)~~ Magnetic susceptibility and geochemical proxies obtained from the high mountain lake record of Laguna Hondera (~~LH~~) evidence humid conditions during the Early Holocene, while a trend towards more arid conditions is recognized since ~7000 cal yr BP, with enhanced Saharan eolian dust deposition until Present. This trend towards enhanced arid conditions was modulated by millennial-scale climate variability. Relative humid conditions occurred during the Iberian Roman Humid Period (2600-1450 cal yr BP) and predominantly arid conditions occurred during the Dark Ages and the Medieval Climate Anomaly (1450-650 cal yr BP). The Little Ice Age (650-150 cal yr BP) is characterized in the LH record by an increase in runoff and a minimum in eolian input. In addition, we further suggest that human impact in the area is noticed through the record of *Olea* cultivation, *Pinus* reforestation and Pb pollution during the Industrial Period (150 cal yr BP-Present). Furthermore, ~~a unique feature preserved at LH is~~ [we estimated that](#) the correlation between Zr and Ca, ~~two important elements of~~ [concentrations stands for](#) Saharan dust ~~source in~~ [input](#) to the Sierra Nevada lake records. ~~This~~ [These assumptions](#) supports ~~that~~ present-day biochemical observations, pointing to eolian input as [the](#) main inorganic nutrient source for oligotrophic mountain lakes. ~~are comparable to the past record of eolian supply to these high altitude lakes.~~

1. Introduction

39 The southern Iberian Peninsula has been the location for a number of recent studies detailing past
40 vegetation and former climate of the region (Carrión et al., 2001, 2003, 2007, 2010; Carrión, 2002;
41 Combourieu Nebout et al., 2009; Jiménez-Espejo et al., 2008; Martín-Puertas et al., 2008, 2010; Fletcher
42 et al., 2010; Nieto-Moreno et al., 2011, 2015; Rodrigo-Gámiz et al., 2011; Moreno et al., 2012 Jiménez-
43 Moreno et al., 2015). Some of these studies have also documented that the western Mediterranean area
44 has been very sensitive to short-term climatic fluctuations throughout the Holocene (e.g., Fletcher and
45 Sánchez-Goñi, 2008; Combourieu Nebout et al., 2009; Fletcher et al., 2010; Jiménez-Moreno et al.,
46 2013). However, a subset of recent studies have attempted to determine how Mediterranean alpine
47 environments have been affected by Holocene climate change through the study of sedimentary records
48 from high elevation wetlands in the Sierra Nevada (Anderson et al., 2011; García-Alix et al., 2012, 2013;
49 Jiménez-Moreno and Anderson, 2012; Jiménez-Moreno et al., 2013; Jiménez-Espejo et al., 2014; Ramos-
50 Román et al., 2016; García-Alix et al., 2017). These alpine lake and bog records show minimal anthropic
51 influence because they are usually elevational higher than major regional Late Holocene human landscape
52 modification. This allows for a potentially clearer climatic signal to be determined from these sites. Even
53 though human impact is less important at high-elevations, the impacts of human activities has also been
54 reconstructed from these Late Holocene sedimentary records (Anderson et al., 2011; García-Alix et al.,
55 2012, 2013; 2017, 2018).

56 Several studies have highlighted the role of atmospheric mineral dust deposition in marine (Pulido-
57 Villena et al., 2008a) and terrestrial (Morales-Baquero et al., 1999; Ballantyne et al., 2011) ecosystem
58 fertilization through major micronutrients supply. Similar results have been described in the Sierra
59 Nevada alpine lakes, where Saharan dust is especially important in conditioning plankton communities
60 from oligotrophic lakes (Morales-Baquero et al., 2006a, 2006b; Mladenov et al., 2008; Pulido-Villena et
61 al., 2008b; Reche et al., 2009). Although this eolian signal has been occasionally recorded in the
62 sedimentary sequences from the Sierra Nevada lakes (Jimenez-Espejo et al., 2014; García-Alix et al.,
63 2017), the record of inorganic nutrients in Saharan dust input in past lake geochemistry has remained
64 elusive. This study investigates a multiproxy sediment core record from Laguna Hondera (LH), located in
65 the Sierra Nevada range with two main goals: (1) identifying and characterizing climatic variability
66 during the Holocene, focusing on vegetation changes, eolian input and runoff sediments variations; and
67 (2) understanding the Saharan dust influence in past lake sedimentation and geochemistry.

68 **2. Study Area**

69 Sierra Nevada is the highest mountain range in the southern Iberian Peninsula. Bedrock of the high
70 elevations of the Sierra Nevada is mostly composed of metamorphic rocks, principally mica schists
71 (Castillo Martín, 2009). During the late Pleistocene, the Sierra Nevada was one of the southernmost
72 mountains to support alpine glaciers and its last advance was recorded during the Little Ice Age (LIA;
73 Palma et al., 2017; Oliva et al., 2018). Subsequently to the melting of ice at the end of the Last Glacial
74 Maximum, wetlands and small lakes formed in the glacial cirque basins, which occur between 2451 and
75 3227 masl (Schulte, 2002; Castillo Martín, 2009; Palma et al., 2017). Several alpine wetland and lakes
76 have been studied in this area during the last few years as shown in Figure 1.

77 2.1. Regional Climate and Vegetation

78 Mediterranean climate characterises southern Iberia, with a marked seasonal variation between warm and
79 dry summers and cool and humid winters (e.g. Lionello et al., 2006). Overprinting this general climate is
80 the influence of the North Atlantic Oscillation (NAO) (Trigo et al., 2004; Trouet et al., 2009). Southern
81 Iberia is also characterized by strong altitudinal contrasts, which in turn controls the precipitation
82 patterns, with mean annual values ranging from $<400 \text{ mm yr}^{-1}$ to $>1400 \text{ mm yr}^{-1}$ in the southeast desert
83 lowlands and the southwest highland, respectively (Jiménez-Moreno et al., 2013 and references therein);
84 ~~demonstrating the complexity of climate regime in this area.~~

85 As with most mountainous regions, species and species groupings in the Sierra Nevada are distributed
86 with respect to elevation, depending on the temperature and rainfall gradients (e.g., El Aallali et al., 1998;
87 Valle, 2003). Above 2800 masl the oromediterranean flora occurs as tundra-like open grassland. The
88 oromediterranean belt (1900—2800 masl) mostly includes dwarf *Juniperus* (juniper); xerophytic
89 shrublands and pasturelands and *Pinus sylvestris* and *P. nigra*. The supramediterranean belt (~1400-1900
90 masl) is characterized by mixed deciduous and evergreen forest species (i.e., evergreen and deciduous
91 *Quercus*, with *Pinus spp.* and others). Mesomediterranean vegetation (600—1400 masl); includes
92 sclerophyllous shrublands and evergreen *Quercus* woodlands. The natural vegetation has been strongly
93 altered by human activities and cultivation in the last centuries, increasing significantly the abundance of
94 *Olea* (olive), due to cultivation at lower altitudes (Anderson et al., 2011, and references therein), and
95 *Pinus* due to reforestation primarily at higher elevations (Valbuena-Carabaña, 2010).

96 2.2. Laguna Hondera

97 Laguna Hondera (hereafter LH; 2899 masl; 37°02.88'N, 3°17.66'W, [lake surface: 0.0053 km²; maximum](#)
98 [depth: 0.8 m; Morales-Baquero et al., 1999](#); Fig. 1) is a small and shallow lake located at the lowest
99 elevation of a set of lakes locally named Cañada de Siete Lagunas, a glacial valley between two of the
100 highest peaks of the mountain range in the Iberian Peninsula: Alcazaba (3366_masl) and Mulhacén (3479
101 masl). LH has a ~~large~~ catchment area of ~~(1.54-6_ha)km²~~, [which is much larger than](#) previously studied
102 [Sierra Nevada wetlands sites in the region](#) (Laguna de Río Seco, LdRS, [0.09-9_ha km²](#); Borreguil de la
103 Caldera, BdIC, [0.62_ha km²](#); Morales-Baquero et al., 1999; Ramos-Román et al., 2016; [Fig 1 for](#)
104 [locations](#)). The lake was reduced to a little pond in the deepest area of the basin when cored in September
105 2012, with a maximum depth of only a few centimetres.

106 LH presently occurs in the oromediterranean vegetation belt (2800_masl) (El Aallali et al., 1998; Valle
107 et al., 2003). The bedrock in the LH basin consists in Paleozoic and Precambrian mica schist with
108 disthene and staurolite of the lower part of the Caldera Formation (Díaz de Federico et al., 1980).

109 3. Methods

110 3.1. Core sampling, lithology and chronology

111 Six sediment cores were recovered from LH with a Livingstone piston corer in September 2012. LH 12-
112 03 (83_cm) was selected for a multi-proxy study because it was the longest core. Cores were wrapped
113 with tin foil and plastic film and transported to Universidad de Granada, where they were stored at 4°C.

114 Core LH 12-03 was split longitudinally and the sediments ~~features were~~ described. ~~The M~~magnetic
115 susceptibility was measured every 0.5 cm with a Bartington MS2E ~~meter~~ in SI units ($\times 10^{-4}$) ~~along the~~
116 ~~entire LH 12-03 core~~ (Fig. 2). The sediment cores were subsampled every 1 cm for ~~different several~~
117 analyses, ~~i.e., one portion for including~~ pollen and ~~another~~ geochemistry ~~analysis~~.

118 The age model was built using seven AMS radiocarbon dates from vegetal remains (Table 1; Fig. 2) by
119 means of Clam software (Blaauw, 2010; version 2.2), which used the IntCal13 curve for radiocarbon age
120 calibration (Reimer et al., 2013). A smooth spline approach was chosen (Fig. 2). The sediment
121 accumulation rate (SAR) was calculated with the average rate from the Clam smooth spline output (Fig.
122 2).

123 3.2. Pollen

124 Pollen analysis was performed on 1 cm³ of sample collected at regular 1 cm interval throughout the first
125 62 cm of the core. Older sediments (from 62 to 82 cm depth) were barren in pollen, and only one interval
126 at 73 cm could be studied (Fig. 2). Pollen extraction included HCl and HF treatment, sieving, and the
127 addition of Lycopodium spores for calculation of pollen concentration (modified from Faegri and Iversen,
128 1989). Sieving was done using a 10- μ m nylon sieve. The resulting pollen residue was suspended in
129 glycerine and mounted on microscope slides. Slides were analysed at 400x magnification counting a
130 minimum of 300 pollen grains, not including the local aquatic species Cyperaceae, Ranunculaceae and
131 ~~Typha~~ *Typha*. An overview of pollen taxa with abundances >1% for core LH 12-03 is plotted using the
132 Tilia ~~software~~ (Grimm, 1993) in Figure 3. The pollen zonation was delimited visually by a cluster
133 analysis ~~constrained by age~~ of taxa abundance >1% using CONISS ~~software~~ (Grimm, 1987) (Fig. 3).
134 ~~Olea were differentiated from others Oleaceae, such as Phillyrea, based on the thicker intine and higher~~
135 ~~size of reticulum in polar vision (Beug, 2004).~~

136 3.3. Geochemical analyses

137 X-ray fluorescence (XRF) Avaatech core scanner®, located at the University of Barcelona, was used to
138 measure light and heavy elements in the LH 12-03 core. An X-ray current of 650 μ A, a 10 second count
139 time and 10 kV X-ray voltage was used for measuring light elements, whereas 1700 μ A X-ray current, 35
140 second count time and 30 kV X-ray voltage was used for heavy elements. Sampling interval for these
141 analyses was every 0.5 cm. For our study only three elements (K, Ca and Ti) have been considered with
142 enough counts to be representative.

143 ~~Chemical composition was also determined on discrete~~ Inductively coupled plasma-optical emission
144 spectrometry (ICP-OES; Perkin-Elmer optima 8300) was used for major element analysis measurements
145 on discrete samples every 2 cm. Prior to analysis, the samples were dried in an oven and digested with
146 HNO₃ and HF. ~~Inductively coupled plasma-optical emission spectrometry (ICP-OES; Perkin Elmer~~
147 ~~optima 8300) was used for major element analysis measurements~~ Blanks and international standards were
148 used for quality control, the analytical accuracy was higher than $\pm 2.79\%$ and 1.89% for 50 ppm
149 elemental concentrations of Al and Ca, respectively, and better than $\pm 0.44\%$ for 5 ppm elemental
150 concentrations of K.

151 Trace element analysis was performed with an inductively coupled plasma mass spectrometry (ICP-MS;
152 Perkin Elmer Sciex Elan 5000). Samples were measured in triplicate through spectrometry using Re and
153 Rh as internal standards. The instrumental error is 2% for elemental concentrations of 50 ppm (Bea,
154 1996). Both ICP-OES and ICP-MS analyses were performed at the Centre for Scientific Instrumentation
155 (CIC), University of Granada, Spain.

156 3.4. Mineralogical analyses

157 Morphological and compositional analyses were performed using scanning electron microscopy (SEM)
158 with an AURIGA model microscope (Carl Zeiss SMT) coupled with energy-dispersive X-ray
159 microanalysis (EDX) and Electron Backscatter Diffraction (EBSD) mode, also at the CIC (University of
160 Granada, Spain). Mineral grains were analysed to determine provenance, in particular those from eolian
161 origin.

162 3.5 Statistical Analysis

163 [R-mode P](#)principal components analysis (PCA) was run on the geochemical dataset using the PAST
164 software (Hammer et al., 2001). PCA identifies hypothetical variables (components) accounting for as
165 much as possible of the variance in multivariate data (Davis, 1986; Harper, 1999). The elements used in
166 the PCA were standardized by subtracting the mean and dividing by the standard deviation (Davis, 1986).
167 Pb was not included in the PCA analysis due to its anthropogenic origin from mining and industrial
168 pollution during the latest Holocene in this area (García-Alix et al., 2013).

169 4. Results

170 4.1. Lithology and magnetic susceptibility

171 The LH 12-03 sediment core consists primarily of peat in the upper ~60 cm, with mostly sand and clay
172 layers below (Fig. 2). Positive MS peaks coincide with the grey clay intervals between 58 and 72 cm. Peat
173 intervals coincide with relatively low MS values. For example, a minimum in MS occurs at 36-48 cm
174 depth, related with a peaty interval with root remains. Near the bottom of the core, between 76 and 80 cm,
175 a sandy oxidized interval occurs.

176 4.2. Chronology and sedimentation rate

177 The age ~~-~~model of LH 12-03 documents that the record spans the last 10800 cal yr BP (Table 1; Fig. 2).
178 Sediment accumulation rates (SAR) were calculated using the average rate from the Clam smooth spline
179 output (Fig. 2). The SAR below ~39 cm is very constant, varying between 0.049 and 0.061 mm yr⁻¹. The
180 SAR increases exponentially to 0.098 mm yr⁻¹ at 22 cm, 0.167 mm yr⁻¹ at ~9 cm and 0.357 mm yr⁻¹ at
181 the core top. Accordingly with the model age and the SAR, resolution of pollen analysis varies between
182 ~40 years per sample in the top of the core and ~120 years per sample in the lower part. The resolution of
183 the geochemical analysis on discrete samples changes between 100 and 400 years per sample, but the
184 geochemical XRF core scanning resolution ranges between 15 and 100 years per sample, providing

185 higher resolution than geochemical data on discrete sample. The MS analyses resolution varies between
186 15 and 100 years per sample.

187 4.3. Pollen

188 Fifty distinct pollen taxa were recognized, but only those with abundance higher than 1% are included in
189 the pollen diagram (Fig. 3). ~~Six~~ Four pollen zones for the LH 12-03 record are identified, using variation
190 in pollen species plotted in Figure 3 and a cluster analysis run through the CONISS software (Grimm,
191 1987).

192 Zone LH-1 (core bottom ~~7000 cal yr BP~~ 2600 cal yr BP) ~~is defined by~~ is subdivided in two subzones.
193 Subzone LH-1A (bottom 4000 cal yr BP) is defined by the alternation between Arboreal Pollen (AP) and
194 herbs. AP is composed primarily of *Pinus*, but also *Quercus*. During the interval from ~9500 to ~7000 cal
195 yr. BP only three samples were analysed, due to the low preservation of pollen in this interval. Pollen in
196 this zone-period is dominated by an alternation between Asteraceae (3-60%) and *Pinus* (5-90%) (Fig. 3).
197 ~~Arboreal pollen (AP), composed primarily of *Pinus*, but also *Quercus*, reaches its maximum occurrence~~
198 ~~(90%) at ~7000 cal yr BP.~~ The highest occurrence of Onagraceae (~10%) is identified ~~takes place~~ in this
199 subzone, and Caryophyllaceae reach high values (~10%) as well. Only minor amounts of graminoids
200 (Poaceae and Cyperaceae) occur during this period.

201 ~~Zone LH 2 (~7000-4000 cal yr BP) is characterized by high percentages of tree species, primarily *Pinus*,~~
202 ~~at the beginning of the zone (~90%), decreasing to ~55% at the upper part of the zone. Between ~7000 to~~
203 ~~~4000, *Pinus* pollen decreases from 90% to ~55%, with a minimum (~30%) at 5000 cal yr BP. *Quercus*~~
204 ~~*Quercus* increase from ~2% at the beginning of the zone to ~10% at the end.~~ The highest percentages of
205 *Betula* (~5%) in the record occurs at this time. Asteraceae pollen decreases (~5-30%) ~~is less than in LH 1,~~
206 but Poaceae increase from <5% ~~at the opening of the subzone~~ to >25%. ~~Caryophyllaceae and Onagraceae~~
207 ~~continue to show relatively high values in this zone (~5% and ~6%, respectively).~~ Cyperaceae occur in
208 high percentages (15%).

209 ~~Zone LH 3~~ The subzone LH-1B (~4000-2600 cal yr BP) is defined primarily by a great increase in
210 Poaceae pollen (to ~60%) (Fig. 3). Other important herbs and shrubs include Asteraceae (5-15%) and
211 Caryophyllaceae (~5%). Other pollen types that increase for the first time in this zone include Ericaceae
212 (~3%), *Artemisia* (~3%) and Ranunculaceae (~2-6%). *Pinus* (~3-25%) and Cyperaceae (0-14%) record a
213 minimum in this zone, and Onagraceae disappear altogether (Fig. 3).

214 ~~Zone LH-24~~ (~2600-1450 cal yr BP) pollen assemblages show high variability ~~in this zone~~. *Pinus* pollen
215 varies between ~80% to ~3% from the onset to the end of the zone. Aquatic pollen such as Cyperaceae
216 (~15%) increases. On the other hand, an increase in herbs such as Asteraceae (~5-70%) occurs along the
217 zone, Poaceae pollen varies between ~7 and 12%.

218 ~~Zone LH-35~~ (~1450-~~150~~600 cal yr BP) is subdivided in two subzones. Subzone 3A (~1450-600 cal yr
219 BP) is characterized by an increase in herbaceous pollen, led by Poaceae (~35% maximum during this
220 zone), Asteraceae (~60% maximum during this zone after ~1000 cal yr BP) and *Artemisia* (~10%), with
221 the resulting decrease in AP. Since this subzone to the Present, *Quercus* pollen is the major component of
222 AP instead of *Pinus*. Cyperaceae also show a decrease, and Ranunculaceae reach ~5%. ~~Zone LH-6 (~~~
223 ~~600 cal yr BP present) is divided in two subzones. LH 6A (~600-150 cal yr BP) Subzone 3B (~600-150~~

224 | [cal yr BP](#) documents an increase in *Olea* (~6%), Poaceae (20%), Caryophyllaceae (7%) and *Artemisia*
225 | (~2-20%). *Pinus* (~2%) and Asteraceae (~20%) decrease in this period. Aquatic and wetland pollen show
226 | a rise (Cyperaceae ~30%, Ranunculaceae ~10%).

227 | ~~LH-6B~~-Zone LH-4 (~ 150 cal yr BP-present) depicts a further increase in *Olea* (~25%), Poaceae (~40%)
228 | and *Artemisia* (~10%).

229 4.4. Sediment composition

230 The XRF-scanning method relies on determining the relative variations on elements composition.
231 | Nevertheless, due to the presence of major variations in organic matter or carbonates ~~makes it important it~~
232 | [is necessary](#) to normalize the measured count in order to obtain an environmentally relevant signal
233 | (Löwemark et al., 2011). Aluminium and titanium normalizations are commonly used to discern possible
234 | fluctuations in the lithogenic fraction (enrichment or depletion of specific elements), particularly in the
235 | terrigenous aluminosilicate sediment fraction (Van der Weijden, 2002; Calvert and Pedersen 2007;
236 | Martinez-Ruiz et al., 2015). For this study, the XRF data were normalized to Ti since Al counts obtained
237 | were very low. Poor detection of Al can be related to either low Al content, or high organic and water
238 | contents that increases radiation absorption and affect the intensity of this light element, among other
239 | possibilities (e.g. Tjallingii et al., 2007).

240 Since data spacing is different between the analyses on discrete samples and the XRF scanner, a linear
241 interpolation was performed with the purpose of equalizing the space of the different time series (150-300
242 years). Afterwards, the mobile average was worked out along the time series (taking into account the five
243 nearest points) in order to easily identify trends by means of smoothing out data irregularities. The
244 obtained data were compared, and both XRF-scanner and discrete sample data showed a good correlation.
245 Consequently, the geochemical proxies displayed higher time resolution than the discrete samples (Table
246 2). Discrete sample and XRF data results are described together in order to simplify this section (Fig. 4).

247 | ~~Zone LH 1 (core bottom ~7000 cal yr BP)~~ [The lower part of the core](#) is typified by maximum values of
248 | K/Al and K/Ti ratios, coinciding with the lowest values in Ca/Al, Ca/Ti and Zr/Al ratios. Pb/Al data show
249 | a stable pattern during this interval. Nevertheless, between 10000 and 9000 cal yr BP and ~8200 cal yr
250 | BP the trends were reversed, with relatively low K/Al, low K/Ti and slightly increasing Zr/Al, Ca/Al and
251 | Ca/Ti ratios. A positive peak in Pb/Al ratio at ~8200 cal yr BP is also observed.

252 | ~~Zone LH 2 (Between ~7000 and ~4000 cal yr BP)~~ [shows](#) a decreasing trend in K/Al and K/Ti ratios, ~~while~~
253 | [occurs along with](#) an increasing trend in Zr/Al, Ca/Al and Ca/Ti ratios ~~occurred~~. The Pb/Al ratio remains
254 | constant throughout this interval.

255 | ~~Zone LH 3 (From ~4000 to ~2600 cal yr BP)~~ ~~documents~~ an increase in Zr/Al, Ca/Al and Ca/Ti ratios, ~~;~~
256 | ~~which reaches a maximum at ~2600 cal yr BP.~~ [is documented.](#) [A maximum in these proxies occurs at](#)
257 | [~2600 cal yr BP.](#) A K/Al and K/Ti minima occurs between ~3000 and ~2600 cal yr BP. The Pb/Al ratio
258 | shows a positive peak at ~2800 cal yr BP.

259 | ~~Zone LH 4 (The interval between ~2600 and ~1450 cal yr BP)~~ is characterized by low Ca/Al, Ca/Ti and
260 | Zr/Al ratios, with relatively high K/Al and K/Ti ratios. The Pb/Al ratio shows a flat pattern, increasing at
261 | ~1500 cal yr BP.

262 | ~~Zone LH 5 (The period between ~1450 and ~650 cal yr BP)~~ depicts higher ratios of Zr/Al, Ca/Al and
263 | Ca/Ti and decreasing ratios of K/Al and K/Ti. A somewhat higher Pb/Al ratio is also registered during
264 | this interval.

265 | ~~Zone LH G6 (~650 cal yr BP present) is divided in two subzones. During the LH G6a subzone, From~~
266 | ~~~650 to ~150~~ low values of Zr/Al and Ca/Ti ratios and minimum values Ca/Al ratio occur. Higher K/Al
267 | and K/Ti values are also observed. The Pb/Al ratio decreases during this interval. From ~150 to the
268 | present, an increase in Zr/Al, Ca/Al, Ca/Ti, K/Ti and a Pb/Al maximum occur. Lower K/Al ratio is
269 | recorded during this ~~zone~~ period.

270 | Several studies have demonstrated that PCA analysis of geochemical data can elucidate the importance of
271 | different geochemical components driving the environmental responses in marine and lacustrine records
272 | (Bahr et al., 2014; Yuan, 2017). We performed a PCA analysis of the LH geochemical data, which
273 | yielded two significant components (Fig. 5). The first principal component (PC1) describes 58% of the
274 | total variance. The main negative loadings for PC1 are Rb, Ba, Al, K, Ca, Mg and Sr, while large positive
275 | loadings correspond to Zr and Rare Earth Elements (REE). The second principal component (PC2)
276 | explains 17% of the total variance. The main negative loading for PC2 are Fe, Ca, Zr, Mg and Lu.
277 | Positive loads correspond to Al, K, Ba, Sr and other elements.

278 | SEM analyses show an alternation between a lithology rich in rock fragments and another rich in organic
279 | remains. Also, diatom frustules, rich in silica, are particularly abundant since ~6300 cal yr BP to Present.
280 | Other minerals such as zircon, rounded quartz and monazite were also identified (Fig. 6).

281 | 5. Discussion

282 | Pollen and geochemical proxies have been widely used for reconstructing vegetation changes and
283 | environmental and climate variations in southern Iberia (e.g. Carrión, 2002; Sánchez-Goñi and Fletcher,
284 | 2008; Anderson et al., 2011; Nieto-Moreno et al., 2011; Jiménez-Moreno and Anderson, 2012; Moreno et
285 | al., 2012; Fletcher and Zielhofer, 2013; Jiménez-Espejo et al., 2014; Ramos-Román et al., 2016).
286 | Variations in the occurrences of arboreal taxa such as *Pinus* and other mesic species (e.g. *Betula*,
287 | *Quercus*), indicating relative humid and warm conditions, and xerophytic species (e.g., Poaceae,
288 | Asteraceae, Amaranthaceae, *Artemisia*), representing aridity, have been useful for reconstructing relative
289 | humidity changes in southern Iberian (e.g. Carrión et al., 2001, 2007, 2010; Anderson et al., 2011;
290 | Jiménez-Moreno and Anderson, 2012; Jiménez-Moreno et al., 2013, 2015; Ramos-Román et al., 2016,
291 | 2018a, 2018b). *Pinus* reach percentages over 80% in our record. This bisaccate pollen grain is favoured
292 | by wind transport and has a larger dispersal area than other tree species, and sometimes might be
293 | overrepresented (Poska and Pidek, 2010; Pérez-Díaz et al., 2016). Nevertheless, LH is located at 2899
294 | masl only 99 m above treeline and the upper boundary of the oromediterranean belt (1900-2800 masl)
295 | where *Pinus sylvestris* is the main tree specie (El Aallali et al., 1998; Valle, 2003). Therefore, this
296 | apparently anomalous high concentration of *Pinus* may be caused by an upward migration of the
297 | oromediterranean belt and treeline towards higher elevations and around the LH during warmer and more
298 | humid periods, which could have been overstated due to its high pollen-production and dispersal.
299 | Therefore, *Pinus* seems to be mostly recording a regional climatic signal, without allocthonous influence.

300 | Over 75% of the total geochemical data variance is explained by the PC1 and PC2 (Fig. 5). We interpret

301 the results of PC1 as resulting from certain sorting between heavy minerals (positive loading; Zr and
302 REE) vs. clay minerals and feldspars (negative loadings; K, Al and Ca). The drainage basin is composed
303 mainly by mica schist, consequently enhanced in K-rich minerals such as mica and feldspar (Díaz de
304 Federico et al., 1980). This sorting between heavy minerals (enriched in Zr and REE) and clays and
305 feldspars (enriched in K and Al) (Fig. 5a), was probably linked to physical weathering within the basin
306 and to resulting runoff until final deposition in the lake.

307 On the other hand, we interpret the results of PC2 as differentiating autochthonous elements (positive
308 loadings) vs. Saharan allochthonous input (negative loadings). In the first case, due to the abundance of
309 mica schist within the LH drainage basin (Díaz de Federico et al., 1980), the K/Al and K/Ti ratios are
310 interpreted as detrital products, and thus a proxy of runoff. In the second case, PC2 negative loading Zr,
311 Ca, Mg and Fe (Fig. 5b) grouped elements that are coherent with Saharan input composition (dolomite,
312 iron oxides and heavy minerals) (Ávila, 1997; Morales-Baquero et al., 2006b; [Moreno et al., 2006](#);
313 Pulido-Villena et al., 2007). In addition, Ca shows a strong positive correlation with Zr since 6300 cal yr
314 BP ($r = -0.57$; $p < 0.05$) supporting an eolian origin of the Ca in LH sediments. [Although we cannot exclude
315 others nearby Ca sources or changes in the source of African dust \(Moreno et al., 2006\), the 85% of dust
316 reaching south Iberia derives from the Sahara \(Morales-Baquero and Pérez-Martínez, 2016; Jiménez et
317 al., 2018\).](#) For instance, enrichment in heavy minerals such as zircon and palygorskite has previously
318 been used as an eolian proxy in the western Mediterranean (e.g., Combourieu Nebout et al., 2002,
319 Rodrigo-Gámiz et al., 2011, 2015). High concentrations of Ca in other lacustrine systems is usually
320 associated with biogenic sources when anti-correlated with terrigenous elements (Yuan, 2017).
321 Nevertheless, elevated Ca in the LH record is linked with detrital elements, as shown by PC1, where Ca is
322 associated with K and Al (Fig. 5a). Therefore Ca/Al and Ca/Ti ratios are used in the LH record as Saharan
323 eolian input proxies.

324 Elemental ratio variations, such as the ratios K/Al and K/Ti indicating fluvial input and the ratios Zr/Al or
325 Zr/Th indicating aridity and eolian input, have been previously interpreted in Alboran Sea [marine records](#)
326 as well as in southern Iberia lake records (Martín-Puertas et al., 2010; Nieto-Moreno et al., 2011, 2015;
327 Rodrigo-Gámiz et al., 2011; Jiménez-Espejo et al., 2014; Martínez-Ruiz et al., 2015; García-Alix et al.,
328 2017, 2018). Thus, the integration of both palynological data and geochemical ratios used as detrital input
329 from LH have allowed the reconstruction of the palaeoclimate and palaeoenvironmental history in Sierra
330 Nevada during the Holocene.

331 **5.1. Holocene palaeoclimate and palaeoenvironmental history**

332 **5.1.1. Early and Mid-Holocene humid conditions (10800–7000 cal yr BP)**

333 The wettest conditions are recorded during the Early Holocene in Sierra Nevada. This is shown in the LH
334 record by the highest K/Al ratio and MS values, and the low values in Zr/Al, Ca/Al and Ca/Ti ratios,
335 suggesting that runoff dominated over eolian processes at this time (zone LH-1; Fig. 7) and agrees with
336 previous studies in the area (Anderson et al., 2011; Jiménez-Moreno and Anderson, 2012; García-Alix et
337 al., 2012; Jiménez-Espejo et al., 2014). Unfortunately, the pollen record from LH during this interval is
338 insufficient to confirm this interpretation, due to the high detrital sediment composition and low organic
339 content, as shown by the low MS values and low pollen preservation. However, high percentages of AP

340 in two out of three analysed samples suggest humid conditions and high runoff during this period, and
341 maybe an upward migration of the oromediterranean belt inferred by the high *Pinus* percentages.

342 An Early Holocene humid stage is noticed in other nearby sites, such as the south-faced Laguna de Río
343 Seco (LdRS; Fig. 1) (Anderson et al., 2011), when the highest lake level of the Holocene occurred. This is
344 also coeval with the dominance of arboreal species such as *Pinus* as well as aquatic and wetland plants
345 (Anderson et al., 2011). Low eolian input, noted by geochemical ratios, is also recorded in LdRS during
346 this interval (Jiménez-Espejo et al., 2014). Further indications of elevated humidity come from the north-
347 facing Borreguil de la Virgen (BdIV) (see Fig. 1), which is dominated by an AP assemblage and a high
348 occurrence of aquatic algae *Pediastrum* along with a higher lake level (Jiménez-Moreno and Anderson,
349 2012).

350 Although the preponderance of evidence accumulated for the Early Holocene suggests overall humid
351 conditions, at least three relatively arid periods are identified with the geochemical data in the LH record
352 (Fig. 7). The first arid period occurred between ~9600 and 9000 cal yr BP, the second occurred ~8200 cal
353 yr BP and the third around 7500 cal yr BP.

354 The first arid event is characterized in LH by a decrease in K/Al and K/Ti ratios and MS, resulting from
355 the lower runoff input with the concomitant change to a more peaty composition. This event could be
356 correlated with a dryness event recorded in the Siles Lake record (Carrion, 2002) at ~9300 cal yr BP
357 noticed by an increase in *Pseudoschizaea*, which was coeval with a minor decrease in arboreal pollen also
358 recorded in several sites in North Iberia (Iriarte-Chiapusso et al., 2016). At marine site ODP 976 (Fig.1;
359 Combourieu-Nebout et al., 2009) a decrease in deciduous *Quercus* occurred between 9500 and 9200 cal
360 yr BP indicating a rapid excursion towards arid conditions (Fig.7). The speleothem record of Corchia
361 Cave also shows dryer conditions during this interval (Fig. 7; Regattieri et al., 2014) In addition, a
362 decrease in fluvial input in the Southern Alps and an aridification phase in southeastern France and
363 southeastern Iberia has been similarly recorded (Jalut et al., 2000).

364 The second dry event recorded at ~8200 cal yr BP is depicted in LH record by a negative peak in K/Ti
365 and K/Al ratios, and by the onset of a trend toward peatier lithology as evidenced by the MS profile. This
366 event is not recognized in LH record as clearly as the 9500 cal yr BP and the 7500 cal yr BP dry events. A
367 decrease in *Pinus* percentage is observed in the nearby LdRS (Anderson et al., 2011), while a forest
368 decrease is recorded in the Alboran Sea sites MD95-2043 and ODP 976. In several records from north
369 western Iberia, a decrease in arboreal pollen also occurred at this time (Iriarte-Chiapusso et al., 2016).

370 The 8.2 ka event was the most rapid climate change towards cooler conditions occurred during the
371 Holocene. It was defined in Greenland ice cores by minimum values in $\delta^{18}O$ and affected the North
372 Atlantic basin and the Mediterranean area (Alley et al., 1997; Rasmussen et al., 2007; Wiersma et al.,
373 2011). Recent simulations point to a fresh water input in North Atlantic which could slow down the North
374 Atlantic Deep Water (NADW) formation preventing the heat transport over the north hemisphere
375 (Wiersma et al., 2010, 2011; Young et al., 2013).

376 Another dry event is recorded in LH at ~7500 cal yr BP evidenced by the higher peat content in the
377 sediment, as well as by the lower MS values and a relative minimum in the K/Ti ratio. A relative AP
378 minimum also occurred in LH at this time. This short-live event is depicted sharper than 8200 cal yr BP
379 event in several sites in southern Iberia and Alboran Sea: In the Padul record, located at 725 masl at the

380 lower part of Sierra Nevada a decrease in both evergreen and deciduous *Quercus* is interpreted as a dry
381 and cold event (Ramos-Román, 2018; Ramos-Román et al., 2018a); forest expansion in Guadiana valley
382 during the early-mid Holocene is interrupted by a xeric shrublands development between 7850 and 7390
383 cal yr BP (Fletcher et al., 2007); in the Alboran Sea a decrease in deciduous *Quercus* is registered at site
384 MD95-2043; at site 300G a decrease in winter and summer temperatures is also recorded during this
385 interval (Jiménez-Espejo et al., 2008); in lake Pergusa (south Italy) a trend toward arid conditions began
386 at ~7500 cal yr BP (Magny et al., 2012); in Corchia Cave an arid excursion occurred at ~7500 cal yr BP
387 within an overall humid period between 8300 cal yr BP and 7200 cal yr BP (Fig. 7; Regattieri et al.,
388 2014).

389 Importantly, these arid events recorded in LH at 9600 to 9000 cal yr BP and 8200 cal yr BP are coeval
390 with the ice-rafted debris events 6 and 5 defined by Bond et al. (1997) in North Atlantic.

391 **5.1.2. Mid- and Late Holocene (~7000 cal yr BP-2600 cal yr BP)**

392 The Middle and Late Holocene in the southern Iberian Peninsula is characterized by a trend towards more
393 arid conditions (Jalut et al., 2009; Anderson et al., 2011; Rodrigo-Gámiz et al., 2011; Jiménez-Moreno
394 and Anderson, 2012; Jiménez-Espejo et al., 2014). In the LH record an abrupt decrease in the MS values
395 indicates a lithological change to more peaty sedimentation at ~7000 cal yr BP. Similarly, a decrease in
396 the K/Al and K/Ti ratios, points to a transition to less humidity and runoff (Fig. 7). *Quercus* percentage
397 increases at this time, partially replacing the *Pinus*, which mainly compose the AP during the record. A
398 progressive increasing trend in eolian input from Sahara (Zr/Al, Ca/Al and Ca/Ti ratios) is observed
399 around 5500-6500 cal yr BP (Fig. 7), also pointing to an increase in aridity in the area. This change
400 coincides with regional increases in the Zr/Th ratio (equivalent to Zr/Al ratio) and *Artemisia* pollen, and
401 with decreases in *Betula* and *Pinus* in the LdRS record (Anderson et al., 2011; Jiménez-Espejo et al.,
402 2014), and in *Pinus* in the BdIV record (Jiménez-Moreno and Anderson, 2012). Rodrigo-Gámiz et al.
403 (2011) and Jiménez-Espejo et al. (2014) observed similar geochemical patterns in western Mediterranean
404 marine records and in LdRS, with a decline in fluvial input, and a decline in surface runoff, respectively.
405 The same pattern is noticed in marine pollen records MD95-2043 and ODP 976 (Fletcher and Sanchez-
406 Goñi, 2008; Combourieu-Nebout et al., 2009; Fig. 7). Contemporaneously, aridity is also suggested from
407 speleothem data around the Mediterranean area: At El Refugio cave, a hiatus in the speleothem growing
408 rate occurred between 7300 and 6100 cal year BP (Walczak et al., 2015), which is coeval with a drop in
409 $\delta^{18}O$ in Soreq (Israel) and Corchia (Italy; CC26; Fig. 1 and 7) caves at 7000 cal yr BP (Bar-Matthews et
410 al., 2000; Zanchetta et al., 2007; Regattieri et al., 2014). Also at ~7000 cal yr BP a decreasing trend in the
411 deciduous/sclerophyllous pollen ratio occurred in southeastern France and Iberia (Jalut et al., 2000) and at
412 continental sites around the Mediterranean Sea (Jalut et al., 2009). In addition, very low lake levels were
413 recorded in the Sahara-Sahel Belt (Liu et al., 2007) and in the Southern Alps (Magny et al., 2002).

414 Enhanced arid conditions are observed in the LH record between 4000 and 2500 cal yr BP, interpreted
415 through a decline in AP, and a Poaceae maximum ~~and a peak in *Artemisia*~~. Also a surface runoff
416 minimum and an increase in eolian input proxies took place between 3500 and 2500 cal yr BP (zone LH-
417 3). In Corchia Cave an arid interval was recorded at ~3100 cal yr BP (Regattieri et al., 2014), coeval with
418 another one observed globally and described by Mayewski et al. (2004) between 3500 and 2500 cal yr

419 BP. Nevertheless, this period is not climatically stable, fluctuations are observed in in K/Ti, K/Al, Ca/Ti,
420 Ca/Al and Zr/Al ratios. Furthermore, peaks in *Quercus* are recorded in LH, LdIM and ODP 976 sites at
421 ~3900 cal yr BP and ~3100 cal yr BP, when AP in LH decreases (Combourieu-Nebout et al., 2009;
422 Jiménez-Moreno et al., 2013). This fact a priori contradictory, could be explained by altitudinal
423 displacements of the tree taxa such as *Quercus* in the oromediterranean belt due to the climatic variability
424 occurred along this interval (Carrión, 2002). During warmer periods, this species would be displaced
425 towards higher elevation and the influence of *Quercus* pollen in Sierra Nevada would be larger, this could
426 explain relative higher *Quercus* percentages in LdIM, LH and also in the ODP 976 record. The same
427 relationship between *Quercus* and *Pinus* is observed comparing the BdlC and Padul records, located
428 closely but with large altitude difference (BdlC ~2992 masl; Padul ~725 masl; Ramos-Román, 2018)
429 where is also likely linked to movements in the oromediterranean belt (Ramos-Román, 2018). These
430 altitudinal displacements of the tree taxa have been previously related to temperature changes in others
431 southern Iberian records, suggesting an ecological niche competition between *Pinus* and *Quercus* species
432 at middle altitudes (see Carrión et al., 2002 for a revision).

433 **5.1.3. Iberian Roman Humid Period (IRHP; ~2600-1450 cal yr BP)**

434 Because there is no consensus in the literature about the chronology for the main climatic stages during
435 the last 2000 years (Muñoz-Sobrinó et al., 2014; Helama et al., 2017), here we follow the chronology
436 proposed by Moreno et al. (2012): Dark Ages (DA, 1450-1050 cal yr BP); Medieval Climate Anomaly
437 (MCA, 1050-650 cal yr BP); and LIA (650-150 cal yr BP). Another climatic stage precedes the DA – the
438 Iberian Roman Humid Period (IRHP, 2600-1600 cal yr BP), originally described by Martín-Puertas et al.
439 (2008). However, in the LH record we have established different IRHP limits (2600-1450), based
440 accordingly to the pollen zonation (Fig. 3), and coinciding with the DA onset defined by Moreno et al,
441 (2012).

442 The IRHP has been described as the wettest period in the western Mediterranean from proxies determined
443 both in marine and lacustrine records during the Late Holocene (Reed et al., 2001; Fletcher and Sanchez-
444 Goñi 2008; Combourieu-Nebout et al., 2009; Martín-Puertas et al., 2009; Nieto-Moreno et al., 2013;
445 Sánchez-López et al., 2016). A relative maximum in AP occurred in the LH record during this time, also
446 indicating forest development and relative high humidity during the Late Holocene in the area (zone LH-
447 4; Fig. 7). This is further supported by high K/Al and K/Ti ratios and MS values, indicating high detrital
448 input in the drainage basin, a minimum in Poaceae and low Saharan eolian input (low Ca/Al, Ca/Ti and
449 Zr/Al ratios) (Fig. 7). Fluvial elemental ratios have also shown an increase in river runoff in Alboran Sea
450 marine records (Nieto-Moreno et al., 2011; Rodrigo-Gámiz et al., 2011). This humid period seems to be
451 correlated with a solar maximum (Solanki et al., 2004) and persistent negative NAO conditions (Olsen et
452 al., 2012), which could have triggered general humid conditions in the Mediterranean. However, in the
453 LH record fluctuation in AP between 2300 and 1800 cal yr BP occurred, pointing to arid conditions at
454 that time. This arid event also seems to show up in BdlC, with a decrease in AP between 2400 and 1900
455 cal yr BP (Ramos-Román et al., 2016) and in Zoñar Lake, with water highly chemically concentrated and
456 gypsum deposition between 2140 and 1800 cal yr BP (Martín-Puertas et al., 2009). In Corchia Cave a
457 rapid excursion towards arid condition is recoded at ~2000 cal yr BP (Regattieri et al., 2014) (Fig.7). [As](#)
458 [we explained in section 5, the apparently anomalous percentages of *Pinus* at this time, could be justified](#)

459 [by an upward migrations of the oromediterranean forest species triggered by higher temperatures and/or](#)
460 [the high pollen-production and dispersal of *Pinus*. Nevertheless, we cannot exclude others factors that](#)
461 [could influence the pollen transport such as the wind energy, mostly controlled by the NAO in the](#)
462 [southern Iberia. A persistent negative NAO phase, as occurred during the IRWP \(Sánchez-López et al.,](#)
463 [2016\), would have triggered more humid conditions and higher westerlies influence over southern](#)
464 [Europe. The higher occurrence of *Pinus* in the surrounding area due to the favourable climatic conditions,](#)
465 [along with the higher wind energy over Sierra Nevada and the characteristics of bissacate pollen, could](#)
466 [have overstate the percentages of *Pinus* in our record.](#)

467 **5.1.4. Dark Ages and Medieval Climate Anomaly (DA, MCA; 1450-650 cal yr BP)**

468 Predominantly arid conditions, depicted by high abundance of herbaceous and xerophytic species and an
469 AP minimum in the LH record, are shown for both DA and MCA (zone LH-5; Fig. 7). This is further
470 supported in this record by an increase in Saharan eolian input Ca/Al, Ca/Ti and Zr/Al ratios, and by a
471 decrease in surface runoff, indicated by the K/Al and K/Ti ratios (zone LH-5; Fig. 7). These results from
472 LH agree with climate estimations of overall aridity modulated by a persistent positive NAO phase during
473 this period (Trouet et al., 2009; Olsen et al., 2012), also previously noted by Ramos-Román et al. (2016)
474 in the area (Fig. 7).

475 Generally arid climate conditions during the DA and the MCA have also been previously described in the
476 LdlM and BdIC records, shown by a decrease in mesophytes and a rise of xerophytic vegetation during
477 that time (Jiménez-Moreno et al., 2013; Ramos-Román et al., 2016). Several pollen records in south and
478 central Iberian Peninsula also indicate aridity during the DA and MCA, for example grassland expanded
479 at Cañada de la Cruz, while in Siles Lake a lower occurrence of woodlands occurred (Carrión, 2002).
480 Also in Cimera Lake low lake level and higher occurrence of xerophytes were recorded (Sánchez-López
481 et al., 2016). Arid conditions were depicted in Zoñar Lake by an increase in *Pistacia* and heliophytes (i.e.,
482 Chenopodiaceae) and lower lake level (Martín-Puertas et al., 2010). Similar climatic conditions were
483 noticed in the marine records MD95-2043 and ODP 976 in the Alboran Sea through decreases in forest
484 (Fletcher and Sánchez-Goñi, 2008; Combourieu-Nebout et al., 2009; Fig. 7). Arid conditions in Basa de
485 la Mora (northern Iberian Peninsula) occurred during this time, characterized by maximum values of
486 *Artemisia*, and a lower development of deciduous *Quercus* and aquatic species such as *Potamogeton*, also
487 indicating low lake water levels (Moreno et al., 2012). Arid conditions were also documented by
488 geochemical data in marine records from the Alboran Sea (Nieto-Moreno et al., 2013, 2015), in the Gulf
489 of Lion and South of Sicily (Jalut et al., 2009). Aridity has also been interpreted for central Europe using
490 lake level reconstructions (Magny, 2004) and in speleothems records in central Italy (Regattieri et al.,
491 2014). [Nevertheless, wetter conditions were recorded during the DA in some records from northern](#)
492 [Iberian Peninsula \(Sánchez-López et al., 2016\). Humid conditions depicted by higher lake level and less](#)
493 [salinity occurred in Arreo Lake \(Corella et al., 2013\). In Sanabria Lake, the dominance of planktonic](#)
494 [diatom *Aulacoseira subborealis* is interpreted as relative humid conditions at that time \(Jambrina-](#)
495 [Enríquez et al., 2014\). This heterogeneity in the climate during the DA is due to the existence of an N-S](#)
496 [humidity gradient in the Iberian Peninsula \(Sánchez-López et al., 2016\). Nonetheless, this gradient seems](#)

497 | [to be more diffuse during the MCA, which is characterized as an overall arid period in the entire Iberian](#)
498 | [Peninsula \(Morellón et al., 2012; Sánchez-López et al., 2016\).](#)

499 **5.1.5. Little Ice Age (LIA; 650-150 cal yr BP)**

500 The LIA is interpreted as an overall humid period in the LH record. This is indicated by higher AP values
501 than during the MCA, low Saharan dust input (low Ca/Al, Ca/Ti and Zr/Al ratios), a decrease in herbs
502 (Poaceae) and high values in the K/Al and K/Ti ratios indicating enhanced runoff (zone LH-6A; Fig. 7).
503 An increase in fluvial-derived proxies has been previously documented in other Iberian terrestrial records
504 such as Basa de la Mora Lake (Moreno et al., 2012), Zoñar Lake (Martín-Puertas et al., 2010) or Cimera
505 Lake (Sánchez-López et al., 2016) and marine records from the Alboran Sea basin (Nieto-Moreno et al.,
506 2011, 2015). Lake level reconstructions in Estanya Lake, in the Pre-Pyrenees (NE Spain), have shown
507 high water levels during this period (Morellón et al., 2009, 2011), supporting our humid climate
508 inferences. Nevertheless, fluctuations in *Artemisia* during the LIA suggest an unstable period in Sierra
509 Nevada (Fig. 8), in agreement with the high variability in *Pinus*, *Artemisia*, and water availability
510 deduced from recent high-resolution studies in the neighbour BdIC and BdIV records (Ramos-Román et
511 al., 2016; García-Alix et al., 2017). The same pattern occurred in several Iberian records (Oliva et al.,
512 2018), revealing that the LIA was not a climatically stable period and many oscillations at short-time
513 scale occurred.

514 A persistently negative NAO phase, although with high variability, occurred during this period (Trouet et
515 al., 2009), which could explain the overall humid conditions observed in southern Europe. As in the Early
516 Holocene arid events, solar variability has been hypothesized as the main forcing of this climatic event
517 (Bond et al., 2001; Mayewski et al., 2004; Fletcher et al., 2013; Ramos-Román et al., 2016).

518 **~~5.1.2.6. Anthropogenic impact in the southern Iberia~~ [Industrial Period \(IP; 150 cal yr BP-Present\)](#)**

519 The IP is characterized by a sharp increase in the Pb/Al ratio in LH record (Fig. 8), suggesting more
520 mining, fossil fuel burning or other human industrial activities (García-Alix et al., 2013, 2017). This is
521 coeval with a rise in AP, which is also related to human activities such as *Olea* commercial cultivation at
522 lower elevations around Sierra Nevada or *Pinus* reforestation in the area (Fig. 7 and 8; Valbuena-
523 Carabaña et al., 2010; Anderson et al., 2011). The same pattern has also been observed in others records
524 from Sierra Nevada (Jiménez-Moreno and Anderson, 2012; García-Alix et al., 2013; Ramos-Román et
525 al., 2016), in Zoñar Lake and the Alboran Sea records (Martín-Puertas et al., 2010). In addition, a
526 progressively increasing trend in Zr/Al and Ca/Al ratios is observed during the last two centuries, which
527 could be related to increasing local aridity and/or anthropogenic desertification, but also with a change in
528 the origin and/or composition of the dust reaching to the lake (Jiménez-Espejo et al., 2014), likely related
529 to the beginning of extensive agriculture and the concomitant desertification in the Sahel region (Mulitza
530 et al., 2010).

531 **5.2. Significance of the eolian record from Laguna Hondera**

532 Saharan dust influence over current alpine lake ecosystems is widely known (Morales-Baquero et al.,
533 2006a, 2006b; Pulido-Villena et al., 2008b; Mladenov et al., 2011, Jiménez et al., 2018). The most

534 representative elements of Saharan dust in LH record are Fe, Zr and Ca as shown by the PC2 loading
535 (Fig. 5), where Ca and Fe directly affect the alpine lake biogeochemistry in this region (Pulido-Villena et
536 al., 2006, 2008b, Jiménez et al., 2018). Zirconium is transported in heavy minerals in eolian dust (Govin
537 et al., 2012) and has largely been used in the Iberian Peninsula and the western Mediterranean as an
538 indicator of eolian Saharan input (Moreno et al., 2006; Nieto-Moreno et al., 2011; Rodrigo-Gámiz et al.,
539 2011; Jiménez-Espejo et al., 2014; Martínez-Ruiz et al., 2015, and references therein). High Zr content
540 has also been identified in present aerosols at high elevations in Sierra Nevada (García-Alix et al., 2017).
541 Considering the low weatherable base cation reserves in LH bedrock catchment area, calcium is
542 suggested to be carried by atmospheric input of Saharan dust into alpine lakes in Sierra Nevada (Pulido-
543 Villena et al., 2006, see discussion; Morales-Baquero et al., 2013). This is the first time that the Ca signal
544 is properly recorded in a long record from Sierra Nevada. This could be explained by higher evaporation
545 rates at this site promoting annual lake desiccation that could prevent Ca water column dissolution and
546 using/recycling by organism, preserving better the original eolian signal. These elements have an essential
547 role as nutrients becoming winnowed and recycled rapidly in the oligotrophic alpine lake ecosystem
548 (Morales-Baquero et al., 2006b). This phenomenon has also been observed in other high-elevation lakes
549 where the phytoplankton is supported by a small and continually recycled nutrient pool (e.g., Sawatzky et
550 al., 2006).

551 The SEM observations further confirm the presence of Saharan dust in the lake sediments from LH and
552 the occurrence of Zircon, the main source of eolian Zr, which is relatively abundant (Fig. 6a). Quartz with
553 rounded morphologies (eolian erosion) are also frequent (Fig. 6b) in the uppermost part of the record as
554 well as REE rich minerals, such as monazite, which is typical from the Saharan-Sahel Corridor area
555 (Moreno et al., 2006) (Fig. 6c). In addition, the fact that the highest correlation between Ca and Zr
556 occurred after ~6300 cal yr BP, ($r=0.57$ $p<0.005$) along with the SEM observation and the low
557 availability of Ca in these ecosystems, could suggest that the beginning of Saharan dust arrivals to the
558 lake, including both elements, took place at this time, giving rise to the present way of nutrient inputs in
559 these alpine lakes (Morales-Baquero et al., 2006b; Pulido-Villena et al., 2006). The onset of Saharan dust
560 input into southern Iberia occurred prior to the end of the African Humid Period (AHP; ~5500 cal yr BP;
561 deMenocal et al., 2000), as previously noticed in the nearby LdRS (Jiménez-Espejo et al., 2014) and in
562 Alboran Sea (Rodrigo-Gámiz et al., 2011). This could suggest a progressive climatic deterioration in
563 North Africa, which culminated with the AHP demise and the massive Saharan dust input recorded in all
564 records in Sierra Nevada at ~3500 cal yr BP (Fig. 7).

565 **6. Conclusions**

566 The multiproxy paleoclimate analysis from LH has allowed the reconstruction of the vegetation and
567 climate evolution in Sierra Nevada and southern Iberia during the Holocene, and the possible factors that
568 have triggered paleoenvironmental changes. Climate during the Early Holocene was predominantly
569 humid, with two relatively arid periods between 10000 [and](#) -9000 and [at](#) ~8200 cal yr BP, resulting in
570 less detrital inputs and a change to more peaty lithology. The onset of an arid trend took place around
571 7000 cal yr BP, decreasing the runoff input in the area. A significant increase in eolian-derived elements

572 occurred between 6300 and 5500 cal yr BP, coinciding with the AHP demise. An arid interval is recorded
573 between 4000 and 2500 cal yr BP, with a vegetation assemblage dominated by xerophytes.
574 Relative humid conditions occurred in the area between 2500 and 1450 cal yr BP, interrupting the Late
575 Holocene aridification trend. This humid interval was characterized by expansion of forest vegetation,
576 high runoff input, and a more clayey lithology. However, during the DA and the MCA (1450-650 cal yr
577 BP) there was enhanced eolian input and an expansion of xerophytes, indicating increased arid
578 conditions. In contrast, the LIA (650-150 cal yr BP) was characterized by predominant humid conditions
579 as pointed out high runoff and low eolian input.
580 ~~The first human impact signals in LH is recorded at ~2800 cal yr BP with a rise of Pb/Al ratio, coinciding~~
581 ~~with the onset of mining in the Iberian Peninsula.~~The IP (150 cal yr BP-Present) is characterized in the
582 LH record by the highest values of the Pb/Al ratio, probably indicating fossil fuel burning by enhanced
583 mining and metallurgy industry. The increase in human activities at this time in this area can also be
584 deduced by the expansion of *Olea* cultivation at lower elevations and *Pinus* reforestation in the area.
585 Importantly, the LH record shows a unique and exceptional Ca signal derived from eolian input (high Ca-
586 Zr correlation) during the past ~6300 years in Sierra Nevada. The good preservation of the Ca record
587 might have been favoured by the high evaporation and the low lake depth, which could have prevented
588 Ca column water dissolution and its re-use by organisms. Our record indicate that present-day inorganic
589 nutrient input from Sahara was established 6300 yrs ago and lasted until the present, with variations
590 depending on the prevailing climate.

591 Acknowledgements

592 This study was supported by the project P11-RNM 7332 of the “Junta de Andalucía”, the projects
593 CGL2013-47038-R, CGL2015-66830-R of the “Ministerio de Economía y Competitividad of Spain and
594 Fondo Europeo de Desarrollo Regional FEDER”, the research groups RNM0190 and RNM179 (Junta de
595 Andalucía). We also thank to Unidad de Excelencia (UCE-PP2016-05). J.M.M.F acknowledges the PhD
596 funding provided by Ministerio de Economía y Competitividad (CGL2015-66830-R) A.G.-A. was also
597 supported by a Marie Curie Intra-European Fellowship of the 7th Framework Programme for Research,
598 Technological Development and Demonstration of the European Commission (NAOSIPUK. Grant
599 Number: PIEF-GA-2012-623027) and by a Ramón y Cajal Fellowship RYC-2015-18966 of the Spanish
600 Government (Ministerio de Economía y Competitividad) and M.R.G. from the Andalucía Talent Hub
601 Program co-funded by the European Union’s Seventh Framework Program (COFUND – Grant
602 Agreement n° 291780) and the Junta de Andalucía. We thank Santiago Fernández, Maria Dolores
603 Hernandez and Antonio Mudarra for their help recovering the core and Inés Morales for the initial core
604 description and MS data. We thank Jaime Frigola (Universitat de Barcelona) for his help with XRF core
605 scanning. We would also like to thank Nathalie Combourieu Nebout, and the two anonymous reviewers
606 for their comments and suggestions, which improved the paper.

607 References

608 Anderson, R. S., Jiménez-Moreno, G., Carrión, J. S., and Pérez-Martínez, C.: Holocene vegetation history
609 from Laguna de Río Seco, Sierra Nevada, southern Spain, *Quaternary Sci. Rev.* 30, 1615-1629,
610 DOI:10.1016/j.quascirev.2011.03.005, 2011.

611 Andrade, A., Valdeolillos, A., and Ruíz-Zapata, B.: Modern pollen spectra and contemporary
612 vegetation in the Paramera Mountain range (Ávila, Spain), *Rev. Palaeobot. Palyno.*, 82, 127-139,
613 DOI:10.1016/0034-6667(94)90024-8, 1994.

614 Ariztegui, D., Asioli, A., Lowe, J. J., Trincardi, F., Vigliotti, L., Tamburini, F., Chondrogianni, C.,
615 Accorsi, C. A., Bandini Mazzanti, M., Mercuri, A. M., Van der Kaars, S., McKenzie, J. A., and Oldfield,
616 F.: Palaeoclimate and the formation of sapropel S1: inferences from Late Quaternary lacustrine and
617 marine sequences in the central Mediterranean region, *Palaeogeogr. Palaeocl.*, 158, 215-240,
618 DOI:10.1016/S0031-0182(00)00051-1, 2000.

619 Aubet, M. E.: *The Phoenicians and the West: Politics, colonies and trade*, Cambridge University Press,
620 Cambridge, 2001.

621 Ávila, A., Queralt-Mitjans, I., and Alarcón, M.: Mineralogical composition of African dust delivered by
622 red rains over northeastern Spain, *J. Geophys. Res.-Atmos.*, 102, 21977-21996, DOI:10.1029/97JD00485,
623 1997.

624 Ballantyne, A. P., Brahney, J., Fernandez, D., Lawrence, C. L., Saros, J., and Neff, J. C.: Biogeochemical
625 response of alpine lakes to a recent increase in dust deposition in the Southwestern US, *Biogeosciences*,
626 8, 2689, DOI:10.5194/bg-8-2689-2011, 2011.

627 Bar-Matthews, M., Ayalon, A., and Kaufman, A.: Timing and hydrological conditions of sapropel events
628 in the Eastern Mediterranean, as evident from speleothems, Soreq cave, Israel, *Chem. Geol.*, 169, 145-
629 156, DOI:10.1016/S0009-2541(99)00232-6, 2000.

630 Bahr, A., Jiménez-Espejo, F. J., Kolasinac, N., Grunert, P., Hernández-Molina, F. J., Röhl, U., Voelker,
631 A. H. L., Escutia, C., Stow, D. A. V., Hodell, D., and Alvarez-Zarikian, C. A.: Deciphering bottom
632 current velocity and paleoclimate signals from contourite deposits in the Gulf of Cádiz during the last 140
633 kyr: An inorganic geochemical approach, *Geochem. Geophys. Geosy.*, 15, 3145-3160,
634 DOI:10.1002/2014GC005356, 2014.

635 Blaauw, M.: Methods and code for 'classical' age-modelling of radiocarbon sequences, *Quat.*
636 *Geochronol.*, 5, 512-518, DOI:10.1016/j.quageo.2010.01.002, 2010.

637 Bea, F.: Residence of REE, Y, Th and U in granites and crustal protoliths: implications for the chemistry
638 of crustal melts, *J. Petrol.*, 37, 521-532, DOI:10.1093/petrology/37.3.521, 1996.

639 [Beug, H. J.: Leitfaden der Pollenbestimmung für Mitteleuropa und angrenzende Gebiete, Fischer,
640 Stuttgart, 2004.](#)

641 Bond, G., Showers, W., Cheseby, M., Lotti, R., Almasi, P., deMenocal, P., Priore, P., Cullen, H., Hajdas,
642 I., and Bonani, G.: A pervasive millennial-scale cycle in North Atlantic Holocene and glacial climates,
643 *Science*, 278, 1257-1266, DOI:10.1126/science.278.5341.1257, 1997.

644 Bond, G., Kromer, B., Beer, J., Muscheler, R., Evans, M., Showers, W., Hoffmann, S., Lotti-Bond, R.,
645 Hajdas, I., and Bonani, G.: Persistent solar influence on North Atlantic climate during the Holocene,
646 *Science*, 294, 2130-2136, DOI:10.1126/science.1065680, 2001.

647 Cacho, I., Grimalt, J. O., and Canals, M.: Response of the Western Mediterranean Sea to rapid climatic
648 variability during the last 50,000 years: a molecular biomarker approach, *J. Marine Syst.*, 33-34, 253-272,
649 DOI:10.1016/S0924-7963(02)00061-1, 2002.

650 Calvert, S. E., and Pedersen, T. F.: Elemental proxies for palaeoclimatic and palaeoceanographic
651 variability in marine sediments: interpretation and application, *Proxies in Late Cenozoic*
652 *Paleoceanography*, Elsevier, Amsterdam, 2007.

653 Carrión, J. S.: Patterns and processes of Late Quaternary environmental change in a montane region of
654 southwestern Europe, *Quaternary Sci. Rev.*, 21, 2047-2066, DOI:10.1016/S0277-3791(02)00010-0, 2002.

655 Carrión, J. S., Munuera, M., Dupré, M., and Andrade, A.: Abrupt vegetation changes in the Segura
656 mountains of southern Spain throughout the Holocene, *J. Ecol.*, 89, 783-797, DOI:10.1046/j.0022-
657 0477.2001.00601.x, 2001.

658 Carrión, J. S., Sánchez-Gómez, P., Mota, J. F., Yll, E. I., and Chaín, C.: Fire and grazing are contingent on
659 the Holocene vegetation dynamics of Sierra de Gádor, southern Spain, *Holocene* 13, 839-849,
660 DOI:10.1191/0959683603hl662rp, 2003.

661 Carrión, J. S., Fuentes, N., González-Sampériz, P., Sánchez Quirante, L., Finlayson, J. C., Fernández, S.,
662 and Andrade, A.: Holocene environmental change in a montane region of southern Europe with a long
663 history of human settlement, *Quaternary Sci. Rev.*, 26, 1455-1475, DOI:10.1016/j.quascirev.2007.03.013,
664 2007.

665 Carrión, J. S., Fernández, S., González-Sampériz, P., Gil-Romera, G., Badal, E., Carrión-Marco, Y.,
666 López-Merino, L., López-Sáez, J. A., Fierro, E., and Burjachs, F.: Expected trends and surprises in the
667 Lateglacial and Holocene vegetation history of the Iberian Peninsula and Balearic Islands, *Rev.*
668 *Palaeobot. Palyno.*, 162, 458-476, DOI:10.1016/j.jaridenv.2008.11.014, 2010.

669 Castillo Martín, A.: *Lagunas de Sierra Nevada*, Universidad de Granada, Granada, 2009.

670 Combourieu Nebout, N., Turon, J. L., Zahn, R., Capotondi, L., Londeix, L., and Pahnke, K.: Enhanced
671 aridity and atmospheric high-pressure stability over the western Mediterranean during the North Atlantic
672 cold events of the past 50 ky, *Geology*, 30, 863-866, DOI:10.1130/0091-
673 7613(2002)030<0863:EAAHP>2.0.CO;2, 2002.

674 Combourieu Nebout, N., Peyron, O., Dormoy, I., Desprat, S., Beaudouin, C., Kotthoff, U., and Marret, F.:
675 Rapid climatic variability in the west Mediterranean during the last 25,000 years from high resolution
676 pollen data, *Clim. Past*, 5, 503-521, DOI:10.5194/cpd-5-671-2009, 2009.

677 Comero, S., Locoro, G., Free, G., Vaccaro, S., De Capitani, L., and Gawlik, B. M.: Characterisation of
678 Alpine lake sediments using multivariate statistical techniques, *Chemometr. Intell. Lab.*, 107(1), 24-30,
679 DOI:10.1016/j.chemolab.2011.01.002, 2011.

680 [Corella, J. P., Stefanova, V., El Anjoumi, A., Rico, E., Giralt, S., Moreno, A., Plata-Monter, A., and](#)
681 [Valero-Garcés, B. L.: A 2500-year multi-proxy reconstruction of climate change and human activities in](#)
682 [northern Spain: the Lake Arreo record, *Palaeogeogr. Palaeoclimatol. Palaeoecol.*, 386, 555-568,](#)
683 [DOI:10.1016/j.palaeo.2013.06.022, 2013.](#)

684 Davis, J. C., and Sampson, R. J.: *Statistics and data analysis in geology*, Wiley, New York, 1986.

685 de Lange, G. J., Thomson, J., Reitz, A., Slomp, C. P., Principato, M. S., Erba, E., and Corselli, C.:
686 Synchronous basin-wide formation and redox-controlled preservation of a Mediterranean sapropel, *Nat.*
687 *Geosci.*, 1, 606-610, DOI:10.1038/ngeo283, 2008.

688 deMenocal, P., Ortiz, J., Guilderson, T., Adkins, J., Sarnthein, M., Baker, L., and Yarusinsky, M.: Abrupt
689 onset and termination of the African Humid Period: rapid climate responses to gradual insolation forcing,
690 *Quaternary Sci. Rev.*, 19, 347-361, DOI:10.1016/S0277-3791(99)00081-5, 2000.

691 Díaz de Federico, A.: *Estudio geológico del Complejo de Sierra Nevada en la transversal del Puerto de la*
692 *Ragua (Cordillera Bética)*, Ph.D. thesis, Universidad de Granada, Granada, 1980.

693 El Aallali, A., López Nieto, J. M., Pérez Raya, F., and Molero Mesa, J.: Estudio de la vegetación forestal
694 en la vertiente sur de Sierra Nevada (Alpujarra Alta granadina), *Itinera Geobot.*, 11, 387-402, 1998.

695 Faegri, K., and Iversen, J.: *Textbook of Pollen Analysis*, Wiley, New York, 1989.

696 Fletcher, W. J., Boski, T., and Moura, D.: Palynological evidence for environmental and climatic change
697 in the lower Guadiana valley, Portugal, during the last 13 000 years, *Holocene*, 17, 481-494,
698 DOI:10.1177/0959683607077027, 2007.

699 Fletcher, W. J., and Sánchez Goñi, M. F.: Orbital- and sub-orbital-scale climate impacts on vegetation of
700 the western Mediterranean basin over the last 48,000 yr, *Quaternary Res.*, 70, 451-464,
701 DOI:10.1016/j.yqres.2008.07.002, 2008.

702 Fletcher, W. J., Sánchez Goñi, M. F., Peyron, O., and Dormoy, I.: Abrupt climate changes of the last
703 deglaciation detected in a Western Mediterranean forest record, *Clim. Past*, 6, 245-264, DOI:10.5194/cp-
704 6-245-2010, 2010.

705 Fletcher, W. J., and Zielhofer, C.: Fragility of Western Mediterranean landscapes during Holocene rapid
706 climate changes, *Catena*, 103, 16-29, DOI:10.1016/j.catena.2011.05.001, 2013.

707 García-Alix, A., Jiménez-Moreno, G., Anderson, R. S., Jiménez-Espejo, F. J., and Delgado-Huertas, A.:
708 Holocene paleoenvironmental evolution of a high-elevation wetland in Sierra Nevada, southern Spain,
709 deduced from an isotopic record, *J. Paleolimnol.*, 48, 471-484, DOI:10.1007/s10933-012-9625-2, 2012.

710 García-Alix, A., Jiménez-Espejo, F. J., Lozano, J. A., Jiménez-Moreno, G., Martínez-Ruiz, F., García
711 Sanjuán, L., Aranda Jiménez, G., García Alfonso, E., Ruiz-Puertas, G., and Anderson, R. S.:
712 Anthropogenic impact and lead pollution throughout the Holocene in Southern Iberia, *Sci. Total Environ.*,
713 449, 451-460, DOI:10.1016/j.scitotenv.2013.01.081, 2013.

714 García-Alix, A., Jimenez Espejo, F. J., Toney, J. L., Jiménez-Moreno, G., Ramos-Román, M. J.,
715 Anderson, R. S., Ruano, P., Queralt, I., Delgado Huertas, A., and Kuroda, J.: Alpine bogs of southern

716 Spain show human-induced environmental change superimposed on long-term natural variations, *Sci.*
717 *Rep.-UK*, 7, 7439, DOI:10.1038/s41598-017-07854-w, 2017.

718 [García-Alix, A., Jiménez-Espejo, F.J., Jiménez-Moreno, G., Toney, J.L., Ramos-Román, M.J., Camuera,](#)
719 [J., Anderson, R.S., Delgado-Huertas, A., Martínez-Ruiz, F., and Queralt, I.: Holocene geochemical](#)
720 [footprint from Semi-arid alpine wetlands in southern Spain, *Sci. Data*, 5, 180024,](#)
721 [DOI:10.1038/sdata.2018.24, 2018.](#)

722 Govin, A., Holzwarth, U., Heslop, D., Ford Keeling, L., Zabel, M., Mulitza, S., Collins, J. A., and
723 Chiessi, C. M.: Distribution of major elements in Atlantic surface sediments (36°N-49°S): imprint of
724 terrigenous input and continental weathering, *Geochem. Geophys. Geosy.*, 13, Q01013,
725 DOI:10.1029/2011GC003785, 2012.

726 Grimm, E. C.: CONISS: a Fortran 77 program for stratigraphically constrained cluster analysis by the
727 method of incremental sum of squares, *Comput. Geosci.*, 13, 13-35, DOI:10.1016/0098-3004(87)90022-
728 7, 1987.

729 Grimm, E.: TILIA: a pollen program for analysis and display, Illinois State Museum, Springfield, 1993.

730 Hammer, Ø., Harper, D. A. T., and Ryan, P. D.: Paleontological Statistics Software Package for
731 Education and Data Analysis, *Palaeontol. electron.*, 4, 1-9, 2001.

732 Harper, D. A. T.: Numerical Palaeobiology, John Wiley & Sons, Chichester, 1999.

733 Helama, S., Jones, P. D., and Briffa, K. R.: Dark Ages Cold Period: A literature review and directions for
734 future research, *Holocene* 27, 1600-1606, DOI: 10.1177/0959683617693898, 2017.

735 Jalut, G., Esteban Amat, A., Bonnet, L., Gauquelin, T., and Fontugne, M.: Holocene climatic changes in
736 the Western Mediterranean, from south-east France to south-east Spain, *Palaeogeogr. Palaeoclimatol.*, 160, 255-
737 290, DOI:10.1016/S0031-0182(00)00075-4, 2000.

738 Jalut, G., Dedoubat, J. J., Fontugne, M., and Otto, T.: Holocene circum-Mediterranean vegetation
739 changes: climate forcing and human impact, *Quatern. Int.*, 200, 4-18, DOI:10.1016/j.quaint.2008.03.012,
740 2009.

741 Jambrina-Enríquez, M., Rico, M., Moreno, A., Leira, M., Bernárdez, P., Prego, R., Recio, C., and Valero-
742 Garcés, B. L.: Timing of deglaciation and postglacial environmental dynamics in NW Iberia: the Sanabria
743 Lake record, *Quaternary Sci. Rev.*, 94, 136-158, DOI:10.1016/j.quascirev.2014.04.018, 2014.

744 [Jiménez, L., Rühland, K. M., Jeziorski, A., Smol, J. P., and Pérez-Martínez, C.: Climate change and](#)
745 [Saharan dust drive recent cladoceran and primary production changes in remote alpine lakes of Sierra](#)
746 [Nevada, Spain, *Glob. Change Biol.*, 24, e139-e158, DOI:10.1111/gcb.13878, 2018.](#)

747 Jiménez-Espejo, F. J., Martínez-Ruiz, F., Rogerson, M., González-Donoso, J. M., Romero, O., Linares,
748 D., Sakamoto, T., Gallego-Torres, D., Rueda Ruiz, J. L., Ortega-Huertas, M., and Perez Claros, J. A.:
749 Detrital input, productivity fluctuations, and water mass circulation in the westernmost Mediterranean Sea
750 since the Last Glacial Maximum, *Geochem. Geophys. Geosy.*, 9, Q11U02, DOI:10.1029/2008GC002096,
751 2008.

752 Jiménez-Espejo, F. J., García-Alix, A., Jiménez-Moreno, G., Rodrigo-Gámiz, M., Anderson, R. S.,
753 Rodríguez-Tovar, F. J., Martínez-Ruiz, F., Giral, S., Delgado-Huertas, A., and Pardo-Igúzquiza, E.:
754 Saharan aeolian input and effective humidity variations over western Europe during the Holocene from a
755 high altitude record, *Chem. Geol.*, 374, 1-12, DOI:10.1016/j.chemgeo.2014.03.001, 2014.

756 Jiménez-Moreno, G., and Anderson, R. S.: Holocene vegetation and climate change recorded in alpine
757 bog sediments from the Borreguiles de la Virgen, Sierra Nevada, southern Spain, *Quaternary Res.*, 77, 44-
758 53, DOI:10.1016/j.yqres.2011.09.006, 2012.

759 Jiménez-Moreno, G., García-Alix, A., Hernández-Corbalán, M. D., Anderson, R. S., and Delgado-
760 Huertas, A.: Vegetation, fire, climate and human disturbance history in the southwestern Mediterranean
761 area during the late Holocene, *Quaternary Res.*, 79, 110-122, DOI:10.1016/j.yqres.2012.11.008, 2013.

762 Jiménez-Moreno, G., Rodríguez-Ramírez, A., Pérez-Asensio, J. N., Carrión, J. S., López-Sáez, J. A.,
763 Villariás-Robles, J. J. R., Celestino-Pérez, S., Cerrillo-Cuenca, E., Ángel León, A., and Contreras, C.:
764 Impact of late-Holocene aridification trend, climate variability and geodynamic control on the
765 environment from a coastal area in SW Spain, *Holocene*, 25, 607-617, DOI:10.1177/0959683614565955,
766 2015.

767 Lionello, P., Malanotte-Rizzoli, P., Boscolo, R., Alpert, P., Artale, V., Li, L., Luterbacher, J., May, W.,
768 Trigo, R., Tsimplis, M., Ulbrich, U., and Xoplaki, E.: The Mediterranean climate: an overview of the
769 main characteristics and issues, *Developments in Earth and Environmental Sciences*, 4, Elsevier,
770 Amsterdam, Netherlands, 1-26, 2006.

771 Liu, Z., Wang, Y., Gallimore, R., Gasse, F., Johnson, T., deMenocal, P., Adkins, J., Notaro, M., Prentice,
772 I. C., Kutzbach, J., Jacob, R., Behling, P., Wang, L., and Ong, E.: Simulating the transient evolution and
773 abrupt change of Northern Africa atmosphere–ocean–terrestrial ecosystem in the Holocene. *Quaternary*
774 *Sci. Rev.*, 26, 1818-1837, DOI:10.1016/j.quascirev.2007.03.002, 2007.

775 Löwemark, L., Chen, H.-F., Yang, T.-N., Kylander, M., Yu, E.-F., Hsu, Y.-W., Lee, T.-Q., Song, S.-R.,
776 and Jarvis, S.: Normalizing XRF-scanner data: a cautionary note on the interpretation of high-resolution
777 records from organic-rich lakes, *J. Asian Earth Sci.*, 40, 1250-1256, DOI:10.1016/j.jseaes.2010.06.002,
778 2011.

779 Magny, M., Miramont, C., and Sivan, O.: Assessment of the impact of climate and anthropogenic factors
780 on Holocene Mediterranean vegetation in Europe on the basis of palaeohydrological records,
781 *Palaeogeogr. Palaeoclimatol.*, 186, 47-59, DOI:10.1016/S0031-0182(02)00442-X, 2002.

782 Magny, M., and Bégeot, C.: Hydrological changes in the European midlatitudes associated with
783 freshwater outbursts from Lake Agassiz during the Younger Dryas event and the early Holocene,
784 *Quaternary Res.*, 61, 181-192, doi:10.1016/j.yqres.2003.12.003, 2004.

785 Magny, M., de Beaulieu, J.-L., Drescher-Schneider, R., Vannièrè, B., Walter-Simonnet, A.-V., Miras, Y.,
786 Millet, L., Bossuet, G., Peyron, O., Brugiapaglia, E., and Leroux, A.: Holocene climate changes in the
787 central Mediterranean as recorded by lake-level fluctuations at Lake Accessa (Tuscany, Italy), *Quaternary*
788 *Sci. Rev.*, 26, 1736-1758, DOI:10.1016/j.quascirev.2007.04.014, 2007.

789 Magny, M., Peyron, O., Sadori, L., Ortu, E., Zanchetta, G., Vannière, B., and Tinner, W.: Contrasting
790 patterns of precipitation seasonality during the Holocene in the south- and north-central Mediterranean, *J.*
791 *Quat. Sci.*, 27, 290-296, DOI:10.1002/jqs.1543, 2012.

792 Martín-Puertas, C., Valero-Garcés, B. L., Mata, M. P., González-Sampériz, P., Bao, R., Moreno, A., and
793 Stefanova, V.: Arid and humid phases in southern Spain during the last 4000 years: the Zonar Lake
794 record, *Cordoba, Holocene*, 18, 907-921, DOI:10.1177/0959683608093533, 2008.

795 Martín-Puertas, C., Valero-Garcés, B. L., Brauer, A., Mata, M. P., Delgado-Huertas, A., and Dulski, P.:
796 The Iberian–Roman Humid Period (2600–1600 cal yr BP) in the Zoñar Lake varve record (Andalucía,
797 southern Spain), *Quaternary Res.*, 71, 108-120, DOI:10.1016/j.yqres.2008.10.004, 2009.

798 Martín-Puertas, C., Jiménez-Espejo, F., Martínez-Ruiz, F., Nieto-Moreno, V., Rodrigo, M., Mata, M. P.,
799 and Valero-Garcés, B. L.: Late Holocene climate variability in the southwestern Mediterranean region: an
800 integrated marine and terrestrial geochemical approach, *Clim. Past*, 6, 807-816, DOI:10.5194/cp-6-807-
801 2010, 2010.

802 Martínez-Ruiz, F., Kastner, M., Gallego-Torres, D., Rodrigo-Gámiz, M., Nieto-Moreno, V., and Ortega-
803 Huertas, M.: Paleoclimate and paleoceanography over the past 20,000 yr in the Mediterranean Sea Basins
804 as indicated by sediment elemental proxies, *Quaternary Sci. Rev.*, 107, 25-46,
805 DOI:10.1016/j.quascirev.2014.09.018, 2015.

806 Mayewski, P. A., Rohling, E. E., Curt Stager, J., Karlén, W., Maasch, K. A., David Meeker, L.,
807 Meyerson, E. A., Gasse, F., van Kreveland, S., Holmgren, K., Lee-Thorp, J., Rosqvist, G., Rack, F.,
808 Staubwasser, M., Schneider, R. R., and Steig, E. J.: Holocene climate variability, *Quaternary Res.* 62,
809 243-255, DOI:10.1016/j.yqres.2004.07.001, 2004.

810 Mladenov, N., Pulido-Villena, E., Morales-Baquero, R., Ortega-Retuerta, E., Sommaruga, R., and Reche,
811 I.: Spatiotemporal drivers of dissolved organic matter in high alpine lakes: Role of Saharan dust inputs
812 and bacterial activity, *J. Geophys. Res.-Biogeo.*, 113, DOI:10.1029/2008JG000699, 2008.

813 Mladenov, N., Sommaruga, R., Morales-Baquero, R., Laurion, I., Camarero, L., Diéguez, M. C.,
814 Camacho, A., Delgado, A., Torres, O., Chen, Z., Felip, M., and Reche, I.: Dust inputs and bacteria
815 influence dissolved organic matter in clear alpine lakes, *Nat. Commun.* 2, 405,
816 DOI:10.1038/ncomms1411, 2011.

817 Morales-Baquero, R., Carrillo, P., Reche, I., and Sánchez-Castillo, P.: Nitrogen-phosphorus relationship
818 in high mountain lakes: effects of the size of catchment basins, *Can. J. Fish. Aquat. Sci.*, 56, 1809-1817,
819 DOI:10.1139/cjfas-56-10-1809, 1999.

820 Morales-Baquero, R., Pulido-Villena, E., and Reche, I.: Atmospheric inputs of phosphorus and nitrogen
821 to the southwest Mediterranean region: Biogeochemical responses of high mountain lakes, *Limnol.*
822 *Oceanogr.*, 51, 830-837, DOI:10.4319/lo.2006.51.2.0830, 2006a.

823 Morales-Baquero R., Pulido-Villena, E., Romera, O., Ortega-Retuerta, E., Conde-Porcuna, J. M., Pérez-
824 Martínez, C., and Reche, I.: Significance of atmospheric deposition to freshwater ecosystems in the
825 southern Iberian Peninsula, *Limnetica*, 25, 171-180, 2006b.

- 826 Morales-Baquero, R., Pulido-Villena, E., and Reche, I.: Chemical signature of Saharan dust on dry and
827 wet atmospheric deposition in the south-western Mediterranean region, *Tellus B*, 65,
828 DOI:10.3402/tellusb.v65i0.18720, 2013.
- 829 Morales-Baquero, R., and Pérez-Martínez C.: Saharan versus local influence on atmospheric aerosol
830 deposition in the southern Iberian Peninsula: Significance for N and P inputs, *Global Biogeochem.*
831 *Cycles*, 30, 501-513, DOI:10.1002/2015GB005254, 2016.
- 832 Moreno, A., Pérez, A., Frigola, J., Nieto-Moreno, V., Rodrigo-Gámiz, M., Martrat, B., González-
833 Sampérez, P., Morellón, M., Martín-Puertas, C., Corella, J. P., Belmonte, A., Sancho, C., Cacho, I.,
834 Herrera, G., Canals, M., Grimalt, J. O., Jiménez-Espejo, F. J., Martínez-Ruiz, F., Vegas-Villarrúbia, T.,
835 and Valero-Garcés, B. L.: The Medieval Climate Anomaly in the Iberian Peninsula reconstructed from
836 marine and lake records, *Quaternary Sci. Rev.*, 42, 16-32, DOI:10.1016/j.quascirev.2012.04.007, 2012.
- 837 Moreno, T., Querol, X., Castillo, S., Alastuey, A., Cuevas, E., Herrmann, L., Mounkaila, M., Elvira, J.,
838 Gibbons, W.: Geochemical variations in aeolian mineral particles from the Sahara–Sahel Dust Corridor.
839 *Chemosphere*, 65, 261-270, DOI:10.1016/j.chemosphere.2006.02.052, 2006.
- 840 Morellón, M., Valero-Garcés, B., Vegas-Vilarrúbia, T., González-Sampérez, P., Romero, O., Delgado-
841 Huertas, A., Mata, P., Moreno, A., Rico, M., and Corella, J. P.: Lateglacial and Holocene
842 palaeohydrology in the western Mediterranean region: the Lake Estanya record (NE Spain), *Quaternary*
843 *Sci. Rev.*, 28, 2582-2599, DOI:10.1016/j.quascirev.2009.05.014, 2009.
- 844 Morellón, M., Valero-Garcés, B., González-Sampérez, P., Vegas-Vilarrúbia, T., Rubio, E., Rieradevall,
845 M., Delgado-Huertas, A., Mata, P., Romero, O., Engstrom, D. R., López-Vicente, M., Navas, A., and
846 Soto, J.: Climate changes and human activities recorded in the sediments of Lake Estanya (NE Spain)
847 during the Medieval Warm Period and Little Ice Age, *J. Paleolimnol.*, 46, 423-452, DOI:10.1007/s10933-
848 009-9346-3, 2011.
- 849 [Morellón, M., Pérez-Sanz, A., Corella, J. P., Büntgen, U., Catalán, J., González-Samprizé, P., González-
850 Trueba, J. J., López-Sáez, J. A., Moreno, A., Pla, S., Saz-Sánchez, M. Á., Scussolini, P., Serrano, E.,
851 Steinhilber, F., Stefanova, V., Vegas-Vilarrúbia, T., and Saz-Sánchez, M. A.: A multi-proxy perspective
852 on millennium-long climate variability in the Southern Pyrenees. *Clim. Past*, DOI:10.5194/cpd-7-3049-
853 2011, 2012.](#)
- 854 Mulitza, S., Heslop, D., Pittauerova, D., Fischer, H. W., Meyer, I., Stuut, J.-B., Zabel, M., Mollenhauer,
855 G., Collins, J.A., Kuhnert, H., and Schulz, M.: Increase in African dust flux at the onset of commercial
856 agriculture in the Sahel region, *Nature*, 466, 226-228, DOI:10.1038/nature09213, 2010.
- 857 Sobrino, C. M., García-Moreiras, I., Castro, Y., Carreño, N. M., de Blas, E., Rodríguez, C. F., Judd, A.,
858 and García-Gil, S., Climate and anthropogenic factors influencing an estuarine ecosystem from NW
859 Iberia: new high resolution multiproxy analyses from San Simón Bay (Ría de Vigo), *Quaternary Sci.*
860 *Rev.*, 93, 11-33, DOI:10.1016/j.quascirev.2014.03.021, 2014.
- 861 Nieto-Moreno, V., Martínez-Ruiz, F., Giralt, S., Jiménez-Espejo, F. J., Gallego-Torres, D., Rodrigo-
862 Gámiz, M., García-Orellana, J., Ortega-Huertas, M., and de Lange, G. J.: Tracking climate variability in

863 the western Mediterranean during the Late Holocene: a multiproxy approach, *Clim. Past*, 7, 1395-1414,
864 DOI:10.5194/cp-7-1395-2011, 2011.

865 Nieto-Moreno, V., Martínez-Ruiz, F., Willmott, V., García-Orellana, J., Masqué, P., and Damsté, J. S.:
866 Climate conditions in the westernmost Mediterranean over the last two millennia: An integrated
867 biomarker approach, *Org. Geochem.*, 55, 1-10. DOI:10.1177/0959683613484613, 2013

868 Nieto-Moreno, V., Martínez-Ruiz, F., Gallego-Torres, D., Giralt, S., García-Orellana, J., Masqué, P.,
869 Sinninghe Damsté, J. S., and Ortega-Huertas, M.: Palaeoclimate and palaeoceanographic conditions in the
870 westernmost Mediterranean over the last millennium: an integrated organic and inorganic approach, *J.*
871 *Geol. Soc. London*, 172, 264-271, DOI:10.1144/jgs2013-105, 2015.

872 Oliva, M., Ruiz-Fernández, J., Barriendos, M., Benito, G., Cuadrat, J. M., Domínguez-Castro, F., García-
873 Ruiz, J. M., Giralt, S., Gómez-Ortiz, A., Hernández, A., López-Costas, O., López-Moreno, J. I., López-
874 Sáez, J. A., Matínez-Cortízar, A., Moreno, A., Prohom, M., Saz, M. A. Serrano, E., Tejedor, E., Trigo, R.,
875 Valero-Garcés, B. and López-Costas, O.: The Little Ice Age in Iberian mountains, *Earth-Sci. Rev.*, 177,
876 175-208, DOI:10.1016/j.earscirev.2017.11.010, 2018.

877 Olsen, J., Anderson, N. J., and Knudsen, M. F.: Variability of the North Atlantic Oscillation over the past
878 5,200 years, *Nat. Geosci.*, 5, 808-812, DOI:10.1038/ngeo1589, 2012.

879 Palma, P., Oliva, M., García-Hernández, C., Ortiz, A. G., Ruiz-Fernández, J., Salvador-Franch, F., and
880 Catarineu, M: Spatial characterization of glacial and periglacial landforms in the highlands of Sierra
881 Nevada (Spain), *Sci. Total Environ.*, 584, 1256-1267, DOI:10.1016/j.scitotenv.2017.01.196, 2017.

882 [Poska, A., and Pidek, I. A.: Pollen dispersal and deposition characteristics of *Abies alba*, *Fagus sylvatica*
883 *and Pinus sylvestris*, Roztocze region \(SE Poland\). *Veg. Hist. Archaeobot.*, 19, 91-101,
884 DOI:10.1007/s00334-009-0230-x, 2010.](#)

885 Pulido-Villena, E., Reche, I., and Morales-Baquero, R.: Significance of atmospheric inputs of calcium
886 over the southwestern Mediterranean region: High mountain lakes as tools for detection, *Global*
887 *Biogeochem. Cy.*, 20, GB2012, DOI:10.1029/2005GB002662, 2006.

888 Pulido-Villena, E., Wagener, T., and Guieu, C.: Bacterial response to dust pulses in the western
889 Mediterranean: Implications for carbon cycling in the oligotrophic ocean, *Global Biogeochem. Cy.*, 22,
890 DOI:10.1029/2007GB003091, 2008a.

891 Pulido-Villena, E., Reche, I., and Morales-Baquero, R.: Evidence of an atmospheric forcing on
892 bacterioplankton and phytoplankton dynamics in a high mountain lake, *Aquat. sci.*, 70, 1-9,
893 DOI:10.1007/s00027-007-0944-8, 2008b.

894 Ramos-Román, M. J., Jiménez-Moreno, G., Anderson, R. S., García-Alix, A., Toney, J. L., Jiménez-
895 Espejo, F. J., and Carrión, J. S.: Centennial-scale vegetation and North Atlantic Oscillation changes
896 during the Late Holocene in the southern Iberia, *Quaternary Sci. Rev.*, 143, 84-95,
897 DOI:10.1016/j.quascirev.2016.05.007, 2016.

898 [Ramos-Román, M. J.: Holocene paleoenvironmental change, climate and human impact in Sierra Nevada,
899 Southern Iberian Peninsula, Ph. D. Thesis, Universidad de Granada, Granada, 2018.](#)

900 | [Ramos-Román, M. J., Jiménez-Moreno, G., Camuera, J., García-Alix, A., Anderson, R. S., Jiménez-](#)
901 | [Espejo, F. J., Sasche, D., Toney, J. L., Carrión, J. S., Webster, C and Yanes, Y.: Millennial-scale cyclical](#)
902 | [environment and climate variability during the Holocene in the western Mediterranean region deduced](#)
903 | [from a new multi-proxy analysis from the Padul record \(Sierra Nevada, Spain\), *Glob. Planet. Change,*](#)
904 | [168, 35-53, DOI:10.1016/j.gloplacha.2018.06.003, 2018a.](#)

905 | Ramos-Román, M. J., Jiménez-Moreno, G., Camuera, J., García-Alix, A., Anderson, R. S., Jiménez-
906 | Espejo, F. J., and Carrión, J. S.: Holocene climate aridification trend and human impact interrupted by
907 | millennial-and centennial-scale climate fluctuations from a new sedimentary record from Padul (Sierra
908 | Nevada, southern Iberian Peninsula), *Clim. Past*, 14, 117-137, DOI:10.5194/cp-14-117-2018, 2018b.

909 | Rasmussen, S. O., Vinther, B. M., Clausen, H. B., and Andersen, K. K.: Early Holocene climate
910 | oscillations recorded in three Greenland ice cores, *Quaternary Sci. Rev.*, 26, 1907-1914,
911 | DOI:10.1016/j.quascirev.2007.06.015, 2007.

912 | Reche, I., Ortega-Retuerta, E., Romera, O., Villena, E. P., Baquero, R. M., and Casamayor, E. O.: Effect
913 | of Saharan dust inputs on bacterial activity and community composition in Mediterranean lakes and
914 | reservoirs, *Limnol. Oceanogr.*, 54, 869-879, DOI:10.4319/lo.2009.54.3.0869, 2009.

915 | Reed, J. M., Stevenson, A. C., and Juggins, S.: A multi-proxy record of Holocene climatic change in
916 | southwestern Spain: the Laguna de Medina, Cádiz, Holocene, 11, 707-719,
917 | DOI:10.1191/09596830195735, 2001.

918 | Reimer, P. J., Bard, E., Bayliss, A., Beck, J. W., Blackwell, P. G., Bronk Ramsey, C., Buck, C. E., Cheng,
919 | H., Edwards, R. L., Friedrich, M., Grootes, P. M., Guilderson, T. P., Hafliðason, H., Hajdas, I., Hatté, C.,
920 | Heaton, T. J., Hoffmann, D. L., Hogg, A. G., Hughen, K. A., Kaiser, K. F., Kromer, B., Manning, S. W.,
921 | Niu, M., Reimer, R. W., Richards, D. A., Scott, M., Southon, J. R., Staff, R. A., Turney, C. S. M., and van
922 | der Plicht, J.: IntCal13 and Marine13 radiocarbon age calibration curves 0-50,000 years cal BP,
923 | *Radiocarbon*, 55, 1869-1887, DOI:10.2458/azu_js_rc.55.16947, 2013.

924 | Regattieri, E., Zanchetta, G., Drysdale, R. N., Isola, I., Hellstrom, J. C., Dallai, L.: Lateglacial to holocene
925 | trace element record (Ba, Mg, Sr) from Corchia cave (Apuan Alps, central Italy): paleoenvironmental
926 | implications, *J. Quat. Sci.*, 29, 381-392, DOI:10.1002/jqs.2712, 2014.

927 | Révillon, S., Jouet, G., Bayon, G., Rabineau, M., Dennielou, B., Hémond, C., and Berné, S.: The
928 | provenance of sediments in the Gulf of Lions, western Mediterranean Sea, *Geochem. Geophys. Geosy.*,
929 | 12, Q08006, DOI:10.1029/2011GC003523, 2011.

930 | Rodrigo-Gámiz, M., Martínez-Ruiz, F., Jiménez-Espejo, F. J., Gallego-Torres, D., Nieto-Moreno, V.,
931 | Romero, O., Ariztegui, D.: Impact of climate variability in the western Mediterranean during the last
932 | 20,000 years: oceanic and atmospheric responses, *Quaternary Sci. Rev.*, 30, 2018-2034,
933 | DOI:10.1016/j.quascirev.2011.05.011, 2011.

934 | Sawatzky, C. L., Wurtsbaugh, W. A., Luecke, C.: The spatial and temporal dynamics of deep chlorophyll
935 | layers in high-mountain lakes: effects of nutrients, grazing, and herbivore recycling as growth
936 | determinants, *J. Plankton Res.*, 28, 65-86, DOI:10.1093/plankt/fbi101, 2006.

- 937 Schulte, L.: Climatic and human influence on river systems and glacier fluctuations in southeast Spain
938 since the Last Glacial Maximum, *Quatern. Int.*, 93-94, 85-100, DOI:10.1016/S1040-6182(02)00008-3,
939 2002.
- 940 Sánchez-López, G., Hernández, A., Pla-Rabes, S., Trigo, R. M., Toro, M., Granados, I., Sáez, A.,
941 Masqué, P., Pueyo, J. J., Rubio-Inglés, M. J., and Giralt, S.: Climate reconstruction for the last two
942 millennia in central Iberia: The role of East Atlantic (EA), North Atlantic Oscillation (NAO) and their
943 interplay over the Iberian Peninsula, *Quaternary Sci. Rev.*, 149, 135-150,
944 DOI:10.1016/j.quascirev.2016.07.021, 2016.
- 945 Settle D. M., and Patterson C. C.: Lead in Albacore: guide to lead pollution in Americans, *Science*, 207,
946 1167-76, DOI:10.1126/science.6986654, 1980.
- 947 Solanki, S. K., Usoskin, I. G., Kromer, B., Schüssler, M., and Beer, J.: Unusual activity of the Sun during
948 recent decades compared to the previous 11,000 years, *Nature*, 431, 1084-1087,
949 DOI:10.1038/nature02995, 2004.
- 950 Tjallingii, R., Röhl, U., Kölling, M., and Bickert, T.: Influence of the water content on X-ray fluorescence
951 core-scanning measurements in soft marine sediments, *Geoch. Geophys. Geosy.*, 8,
952 DOI:10.1029/2006GC001393, 2007.
- 953 Trigo, R. M., and Palutikof, J. P.: Precipitation scenarios over Iberia: a comparison between direct GCM
954 output and different downscaling techniques, *J. Climate*, 14, 4442-4446, DOI:10.1175/1520-
955 0442(2001)014<4422:PSOIAAC>2.0.CO;2, 2001.
- 956 Trigo, R. M., Pozo-Vázquez, D., Osborn, T. J., Castro-Díez, Y., Gámiz-Fortis, S., and Esteban-Parra, M.
957 J.: North Atlantic Oscillation influence on precipitation, river flow and water resources in the Iberian
958 Peninsula, *Int. J. Climatol.*, 24, 925-944, DOI:10.1002/joc.1048, 2004.
- 959 Trouet, V., Esper, J., Graham, N. E., Baker, A., Scourse, J. D., and Frank, D. C.: Persistent positive North
960 Atlantic Oscillation mode dominated the Medieval Climate Anomaly, *Science*, 324, 78-80,
961 DOI:10.1126/science.1166349, 2009.
- 962 Valbuena-Carabaña, M., López de Heredia, U., Fuentes-Utrilla, P., González-Doncel, I., and Gil, L.:
963 Historical and recent changes in the Spanish forests: a socioeconomic process, *Rev. Palaeobot. Palyno.*,
964 162, 492-506, DOI:10.1016/j.revpalbo.2009.11.003, 2010.
- 965 Valle, F.: *Mapa de series de vegetación de Andalucía 1: 400 000*, Editorial Rueda, Madrid, 2003.
- 966 Van der Weijden, C. H.: Pitfalls of normalization of marine geochemical data using a common divisor,
967 *Mar. Geol.*, 184, 167-187, DOI:10.1016/S0025-3227(01)00297-3, 2002.
- 968 Walczak, I. W., Baldini, J. U., Baldini, L. M., McDermott, F., Marsden, S., Standish, C. D., Richards, D.
969 A., Andreo, B., and Slater, J.: Reconstructing high-resolution climate using CT scanning of unsectioned
970 stalagmites: A case study identifying the mid-Holocene onset of the Mediterranean climate in southern
971 Iberia, *Quaternary Sci. Rev.*, 127, 117-128, DOI:10.1016/j.quascirev.2015.06.013, 2015.

972 Wanner, H., Brönnimann, S., Casty, C., Gyalistras, D., Luterbacher, J., Schmutz, C., Stephenson, D. B.,
973 and Xoplaki, E.: North Atlantic Oscillation–concepts and studies, *Surv. Geophys.*, 22, 321-381,
974 DOI:10.1023/A:1014217317898, 2001.

975 Wiersma, A. P., and Jongma, J. I.: A role for icebergs in the 8.2 ka climate event, *Climate dynamics*, 35,
976 535-549, DOI:10.1007/s00382-009-0645-1, 2010.

977 Wiersma, A. P., Roche, D. M., and Renssen, H.: Fingerprinting the 8.2 ka event climate response in a
978 coupled climate model, *J. Quat. Sci.*, 26, 118-127, DOI:10.1002/jqs.1439, 2011.

979 Yuan, F.: A multi-element sediment record of hydrological and environmental changes from Lake Erie
980 since 1800, *J. Paleolimnol.*, 58, 23-42, DOI:10.1007/s10933-017-9953-3, 2017.

981 Zanchetta, G., Drysdale, R. N., Hellstrom, J. C., Fallick, A. E., Isola, I., Gagan, M. K., Pareschi, M. T.:
982 Enhanced rainfall in the Western Mediterranean during deposition of sapropel S1: stalagmite evidence
983 from Corchia cave (Central Italy), *Quaternary Sci. Rev.*, 26, 279-286,
984 DOI:10.1016/j.quascirev.2006.12.003, 2007.

985

986

987

988

989

990

991

992

993

994

995

996

997

998

999

1000

1001

1002

1003

1004 **List of tables**

<i>Lab Number</i>	<i>Depth (cm)</i>	<i>Dating Method</i>	<i>Age (14C yr BP±1σ)</i>	<i>Calibrated age (cal yr BP)2σ ranges</i>
	0	Present	2012 CE	-63
<i>Poz-72421</i>	7	14C	40±40	29-139
<i>D-AMS 008539</i>	22	14C	1112±32	935-1078
<i>D-AMS 008540</i>	39	14C	2675±30	2750-2809
<i>BETA-411994</i>	44	14C	3350±30	3550-3643
<i>BETA-411995</i>	55.5	14C	5480±30	6261-6318
<i>Poz-72423</i>	57.5	14C	5510±50	6266-6405
<i>Poz-72424</i>	62	14C	6450±50	7272-7433
<i>Poz-72425</i>	74	14C	8620±70	9479-9778

1005 **Table 1.** Age data for LH 12-03 record. All ages were calibrated using IntCal13 curve (Reimer et al.,
 1006 2013) with Clam program (Blaauw, 2010; version 2.2).

1007

1008

1009

1010

1011

1012

1013

1014

1015

1016

1017

1018

1019

1020

1021

1022

1023

1024

	Simulation							
Correlation	A		B		C		D	
Ca/Ca (XRF)	0.63	p<0.01	0.50	p<0.01	0.57	p<0.01	0.54	p<0.01
K/K (XRF)	0.53	p<0.01	0.64	p<0.01	0.56	p<0.01	0.65	p<0.01

1025 **Table 2.** Simulation of proxy correlation. A) regular interpolation of 300 years sampling spacing. B)
1026 regular interpolation of 300 years sampling spacing and 5 data points moving average. C) regular
1027 interpolation of 150 years sampling spacing. D) regular interpolation of 150 years sampling spacing and 5
1028 data point moving average.

1029

1030

1031

1032

1033

1034

1035

1036

1037

1038

1039

1040

1041

1042

1043

1044

1045

1046

1047

1048

1049

1050

1051

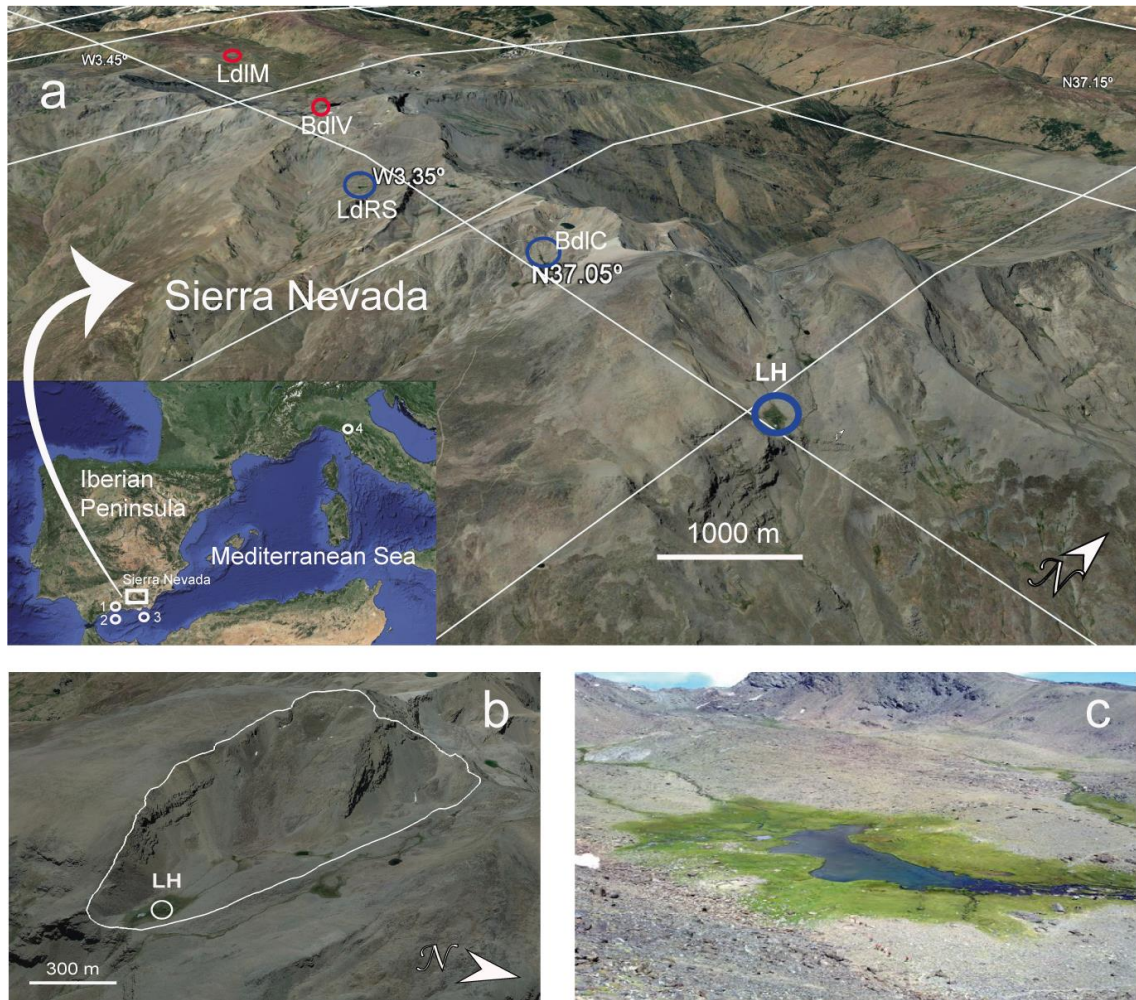
1052

1053

1054

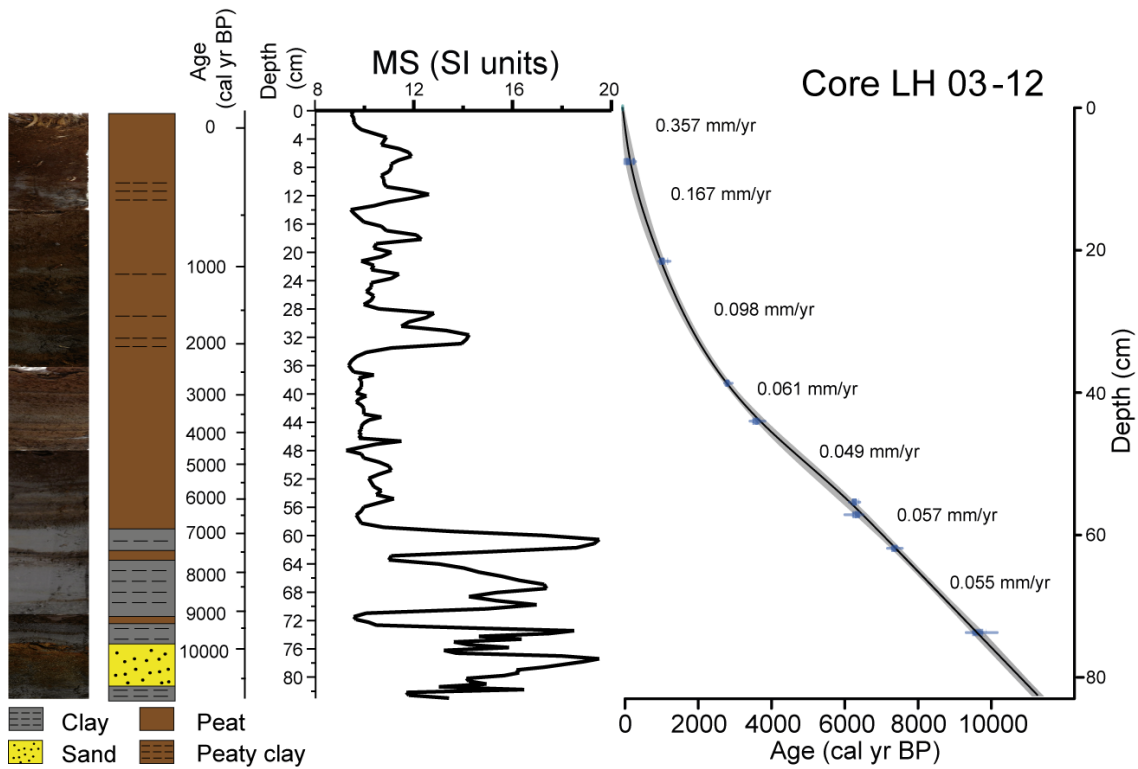
1055

1056



1058

1059 **Figure 1.** (a) Location of the Laguna Hondera (LH) in Sierra Nevada, southern Iberian Peninsula,
 1060 **Mediterranean region**, along with other nearby records mentioned in the text. (1) El Refugio Cave
 1061 stalagmite record (Walczak et al., 2015); (2) ODP 976 pollen record (Combourieu-Nebout et al., 2009);
 1062 (3) MD95-2043 pollen record (Fletcher and Sánchez-Goñi, 2008); (4) CC26, Corchia Cave stalagmite
 1063 record (Zanchetta et al., 2007; Regattieri et al., 2014). Sierra Nevada north-facing sites are encircled in
 1064 red, south-facing sites are encircled in blue. LH: Laguna Hondera, the current study, is shown in bold.
 1065 LdLM: Laguna de la Mula (Jiménez-Moreno et al., 2013); BdLV: Borreguil de la Virgen (García-Alix et
 1066 al., 2012; Jiménez-Moreno and Anderson, 2012); LdRS: Laguna de Río Seco (Anderson et al., 2011;
 1067 García-Alix et al., 2013; Jiménez-Espejo et al., 2014); BdLC: Borreguil de la Caldera (Ramos-Román et
 1068 al., 2016; García-Alix et al., 2017) (b) Regional satellite photo of LH. The white line indicates the
 1069 catchment area. (c) Photo of Laguna Hondera in September 2012, when the core was taken. Photo taken
 1070 by Gonzalo Jiménez-Moreno. [For the coloured figure, we refer the reader to the web version of this](#)
 1071 [article.](#)



1072

1073

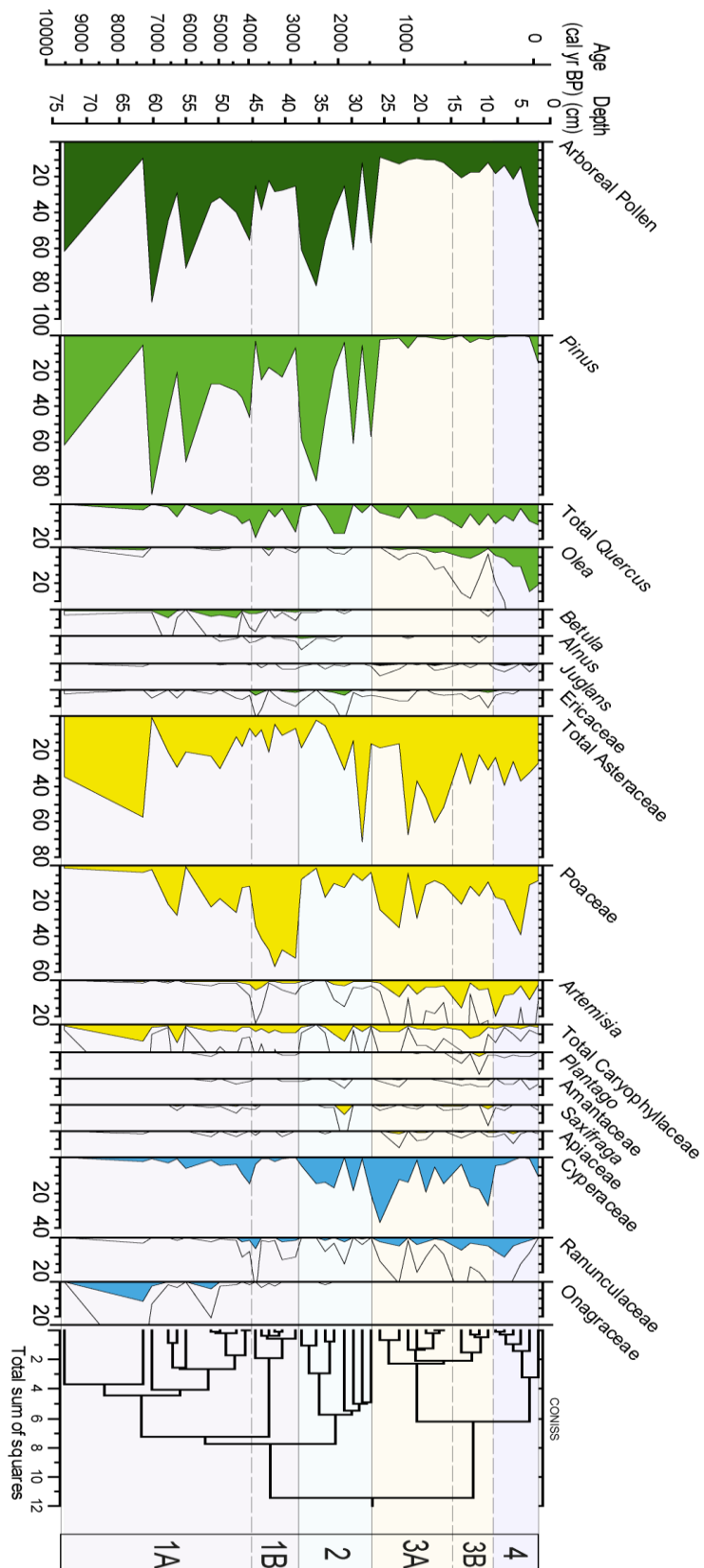
Figure 2. Photo of core LH 12-03, along with the lithology, magnetic susceptibility (MS, in SI units) profile and age-depth model. Sediment accumulation rates (SAR in mm yr⁻¹) are shown between individual radiocarbon ages, [the grey shadow represent the plus/minus range](#) (see details in text for method of construction).

1074

1075

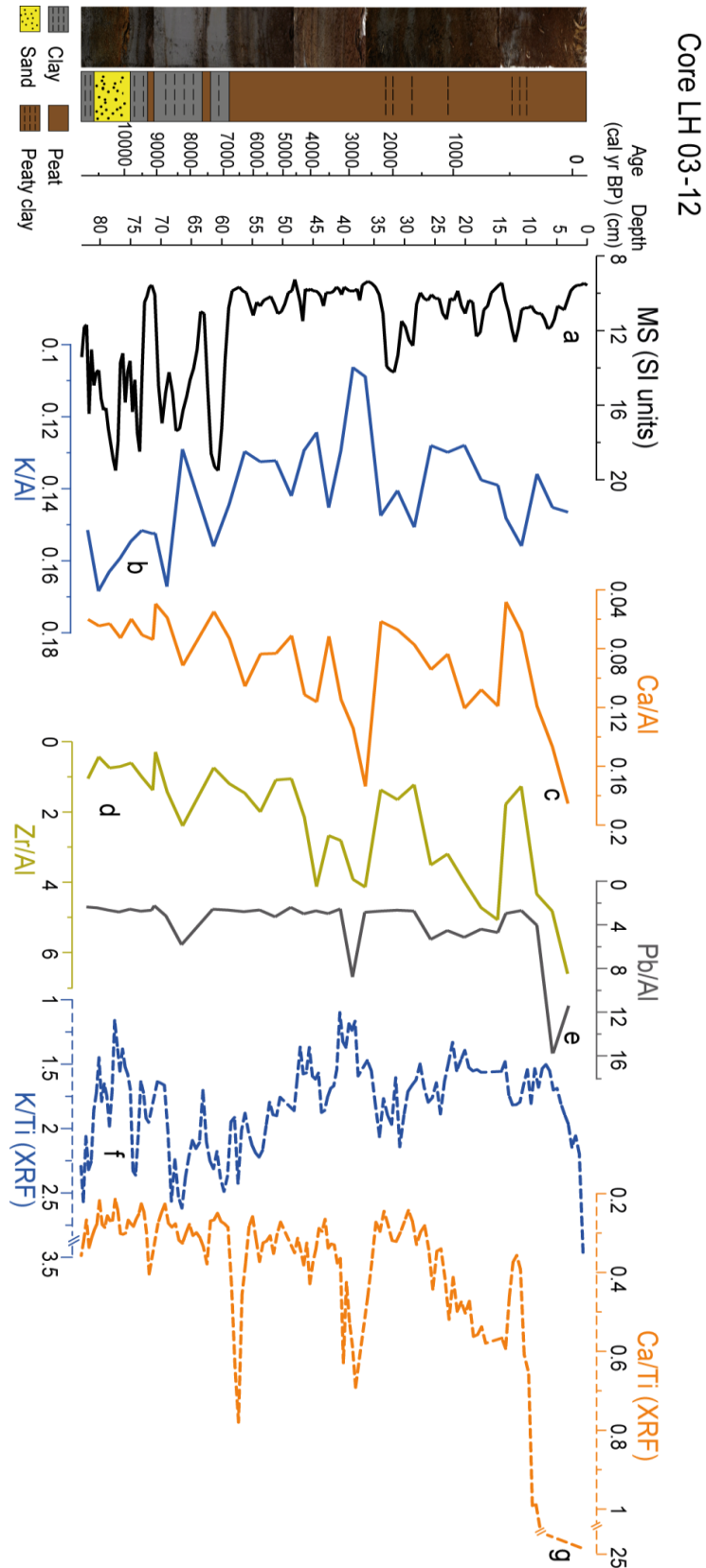
1076

1077



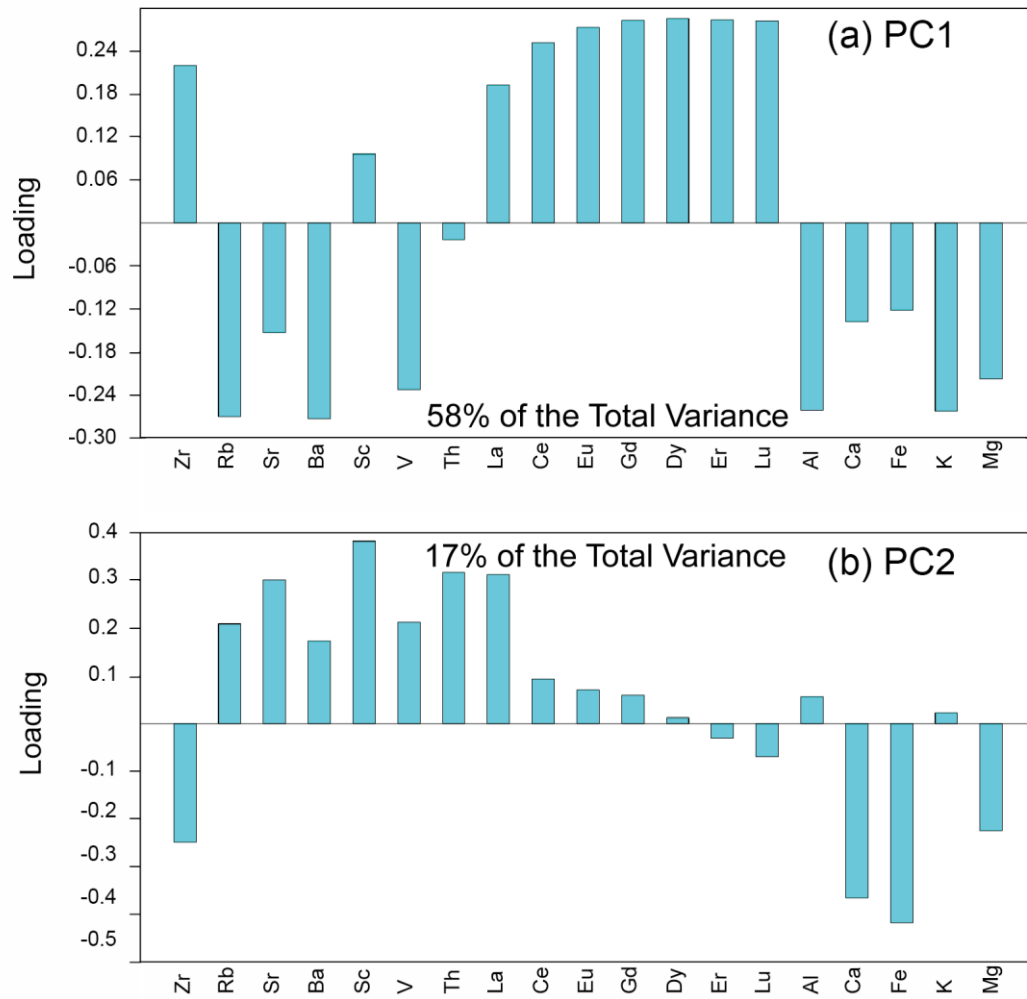
1078

1079 **Figure 3.** Pollen percentage diagram of the LH 12-03 record showing major selected taxa. Major tree
 1080 species are shown in green; shrubs and herbs are shown in yellow; and wetland and aquatic types are in
 1081 blue. Pollen was graphed with the Tilia software (Grimm, 1993), and zoned using the CONISS cluster
 1082 analysis program (Grimm, 1987).



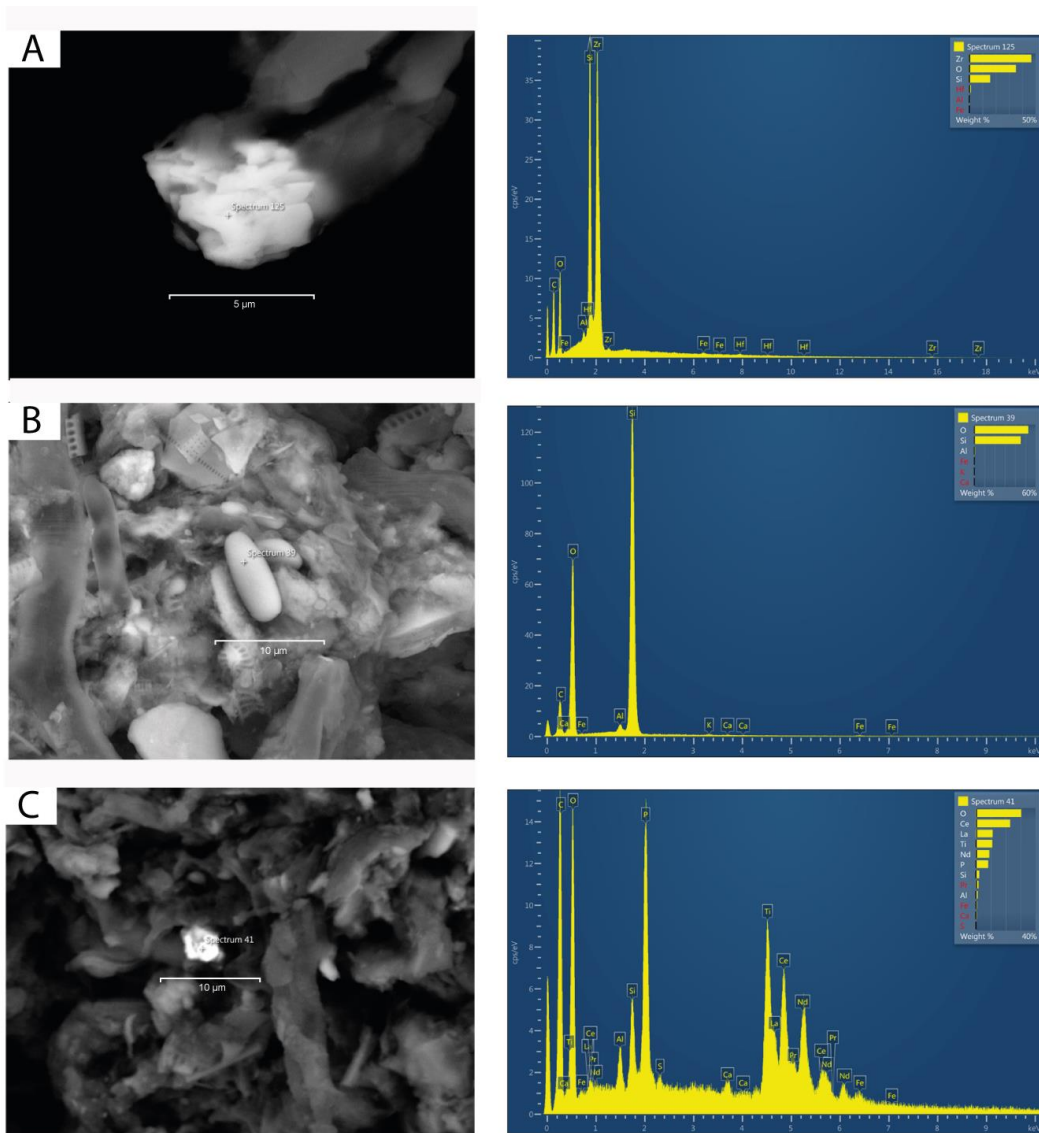
1083

1084 **Figure 4.** Detailed geochemical diagram of the LH 12-03 record showing the selected proxies: (a)
 1085 [Magnetic Susceptibility \(MS\)](#); (b) K/Al; (c) Ca/Al; (d) Zr/Al; (e) Pb/Al; (f) K/Ti (XRF); (g) Ca/Ti (XRF)
 1086 (MS in SI units, Zr/Al and Pb/Al scale $\times 10^{-4}$ and XRF in counts). ~~Pollen zonation described in section 4.3~~
 1087 ~~was used.~~



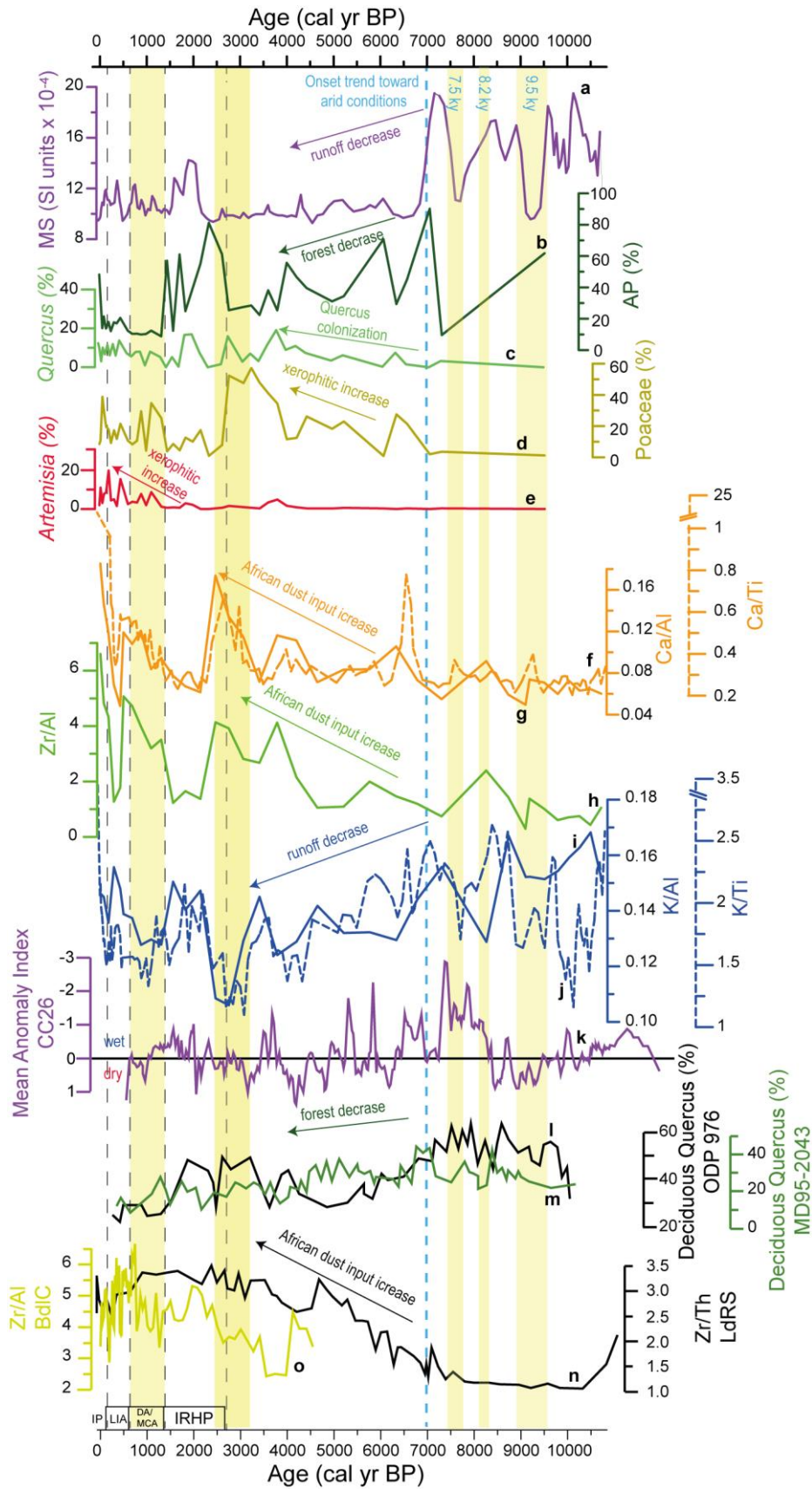
1088

1089 **Figure 5.** Principal Component Analysis (PCA) loadings from selected geochemical elements. (a) PC1,
 1090 which describes 58% of total variance; (b) PC2, which describes 17% of total variance.



1091

1092 **Figure 6.** Electron Backscatter Diffraction microphotographs of the LH 12-03 record with clearer colours
 1093 representing heavier minerals. (a) Zircon, with high Zr content; (b) rounded quartz related with eolian
 1094 transport; (c) monazite, with high REE content.



1095

1096 | **Figure 7.** Comparison between the [Magnetic Susceptibility](#) (MS) data (in SI units $\times 10^{-4}$), the most
 1097 | important pollen taxa and geochemical proxies from LH 12-03 record, with nearby paleoclimate records.
 1098 | (a) [LH Magnetic Susceptibility](#) (MS) from LH 12-03 record; (b) Arboreal Pollen (AP) percentage from

1099 | [LH 12-03 ~~LH~~record](#); (c) *Quercus* percentage from [LH 12-03 ~~LH~~record](#); (d) Poaceae percentage from [LH](#)
1100 | [12-03 ~~LH~~record](#); (e) ~~*Artemisia*~~ *Artemisia* percentage from [LH 12-03 ~~LH~~record](#); (f) Ca/Ti (XRF) ratio
1101 | from [LH 12-03 ~~LH~~record](#) in dashed line; (g) Ca/Al ratio from [LH 12-03 record ~~LH~~](#); (h) Zr/Al ratio from
1102 | [LH 12-03 record~~LH~~](#); (i) K/Al ratio from [LH 12-03 ~~LH~~](#); (j) K/Ti (XRF) ratio from [LH 12-03 ~~LH~~](#) in dashed
1103 | line; (k) Mean Anomaly Index from CC26 [record](#) (Corchia cave; Regattieri et al., 2014); (l) Deciduous
1104 | *Quercus* from ODP 976 [record](#) (Alboran Sea; Combourieu-Nebout et al., 2009); (m) Deciduous *Quercus*
1105 | from MD95-2043 [record](#) (Alboran Sea; Fletcher and Sanchez-Goñi, 2008); (n) Zr/Th ratio from Laguna
1106 | de Río Seco (LdRS) (Jiménez-Espejo et al., 2014; García-Alix et al., 2018); (o) Zr/Al ratio from
1107 | Borreguil de la Caldera (BdlC) (García-Alix et al., 2017; 2018). Yellow bands indicate more arid
1108 | intervals. Dark dashed lines are used for separating the different Current Era periods: IRHP: Iberian
1109 | Roman Humid Period; DA: Dark Ages; MCA: Medieval Climate Anomaly; LIA: Little Ice Age; IP:
1110 | Industrial Period. Blue dashed line indicates the onset of the trend toward arid conditions.

1111

1112

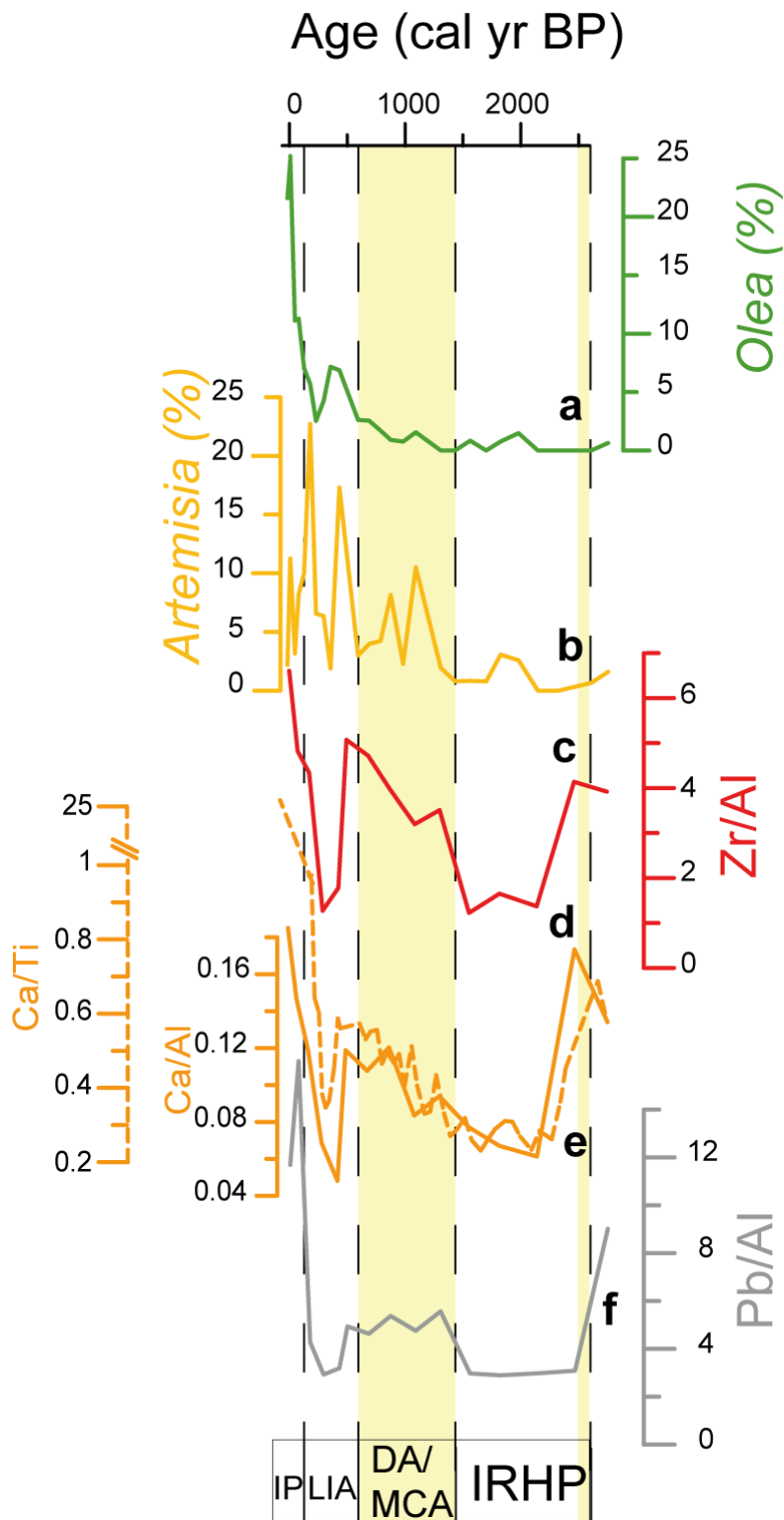
1113

1114

1115

1116

1117



1118

1119 **Figure 8.** Comparison of geochemical proxies with pollen taxa, related to anthropogenic impact for the
 1120 last ~2600 cal yr BP from LH 12-03 record. (a) *Olea* percentage from LH 12-03 record; (b) *Artemisia*
 1121 percentage from LH 12-03 record; (c) Zr/Al ratio from LH 12-03 record; (d) Ca/Al ratio from LH 12-03
 1122 record; (e) Ca/Ti (XRF) ratio from LH 12-03 record; (f) Pb/Al ratio from LH 12-03 record. Yellow bands
 1123 indicate more arid intervals. Dark dashed lines are used for separating the different Current Era periods:

1124 IRHP: Iberian Roman Humid Period; DA: Dark Ages; MCA: Medieval Climate Anomaly; LIA: Little Ice
1125 Age; IP: Industrial Period.